

# Unique miR775-*GALT9* module regulates leaf senescence in *Arabidopsis* during post-submergence recovery by modulating Ethylene and Abscisic acid pathway

Vishnu Mishra<sup>\$1</sup>, Archita Singh<sup>\$1,2</sup>, Nidhi Gandhi<sup>1</sup>, Shabari Sarkar Das<sup>3</sup>, Sandeep Yadav<sup>1</sup>, Ashutosh Kumar<sup>1</sup>, and Ananda K. Sarkar<sup>\*1,2</sup>

<sup>\$</sup>These authors contributed equally to this work.

<sup>1</sup>National Institute of Plant Genome Research, Aruna Asaf Ali Marg, New Delhi, India, 110067.

<sup>2</sup>School of Life Sciences, Jawaharlal Nehru University, New Delhi 110067.

<sup>3</sup>Department of Botany and Forestry, Vidyasagar University, Midnapore, West Bengal 721104 India.

**\*Corresponding author:** Ananda Kumar Sarkar

National Institute of Plant Genome Research (on lien),

Aruna Asaf Ali Marg, New Delhi, India, 110067.

Telephone: +91-11-26735220.

Fax: +91-11-26741146.

Email: aksarkar@nipgr.ac.in

Current Address: School of Life Sciences, Jawaharlal Nehru University, New Delhi 110067.

Email: aksarkar.jnu@gmail.com or anandaksarkar@mail.jnu.ac.in

## Summary statement

Unique miR775-*GALT9* regulates post-submergence recovery by modulating the expression of senescence associated genes (SAGs), ethylene and ABA pathway which provide important insight into a general basic plant response towards submergence.

## Abstract

Submergence-induced hypoxic condition negatively affects the plant growth and development, and causes early onset of senescence. Hypoxia alters the expression of a number of microRNAs (miRNAs). However, the molecular function of submergence stress-induced miRNAs in physiological or developmental changes and recovery remains poorly understood. Here we show that miR775 is an *Arabidopsis thaliana*-specific young and unique miRNA that possibly evolved non-canonically. miR775 post-transcriptionally regulates *Galactosyltransferase (GALT9)* and their expression is inversely affected at 24 hours of complete submergence stress. The overexpression of miR775 (miR775-Oe) confers enhanced recovery from submergence stress and reduced accumulation of *RBOHD* and ROS, in contrast to wild type and *MIM775 Arabidopsis* shoot. A similar recovery phenotype of *galt9* mutant indicates the role of miR775-*GALT9* module in post-submergence recovery. We predicted Golgi-localized *GALT9* to be potentially involved in protein glycosylation. The altered expression of senescence-associated genes (*SAG12*, *SAG29*, and *ORE1*), ethylene signalling (*EIN2* and *EIN3*) and ABA biosynthesis (*NCED3*) pathway genes in miR775-Oe, *galt9* and *MIM775* plants. Thus, our results indicate the role of miR775-*GALT9* module in post-submergence recovery through a crosstalk with ethylene and ABA pathway.

**Keywords:** miRNA, miR775, *GALT9*, senescence, submergence stress, hypoxia, *SAGs*, *Arabidopsis*.

## Introduction:

Abiotic factors like light, temperature, water, oxygen, nutrition, etc. act as external cues to modulate plant growth and development. Globally, flood is one of the major stresses that lead to severe loss in crop yield and productivity (Ismail, 2018, Kumar and Dash, 2019, Bui *et al.*, 2020). Flooding stress is divided into two categories depending upon the water exposure such as, complete submergence, and partial submergence or waterlogging. Under complete submergence, the whole plant is fully immersed in water, while under partial submergence; the shoot terminal is maintained above the water surface (Fukao *et al.*, 2019). Premature senescence, necrosis, and chlorosis, cessation of growth are the major consequences of submergence stress (Zhang *et al.*,

2000, Visser *et al.*, 2003). Submergence initiates various molecular cascades that adversely affect plant growth and development. Submergence also leads to excessive reactive oxygen species (ROS) production and cell death due to the reduced availability of oxygen (hypoxic conditions). Prolonged submergence gradually affects gaseous exchange which leads to cell damage and chlorophyll breakdown causing early onset of senescence (Fukao *et al.*, 2019). *RESPIRATORY BURST OXIDASE HOMOLOGUE D (RBOHD)* is one of the NAPDH oxidases involved in the production of ROS and is widely used as a marker gene to access the ROS accumulation during submergence stress. *RBOHD* promotes the expression of alcohol dehydrogenase (ADH), pyruvate decarboxylase 1 (PDC), lactate dehydrogenase (LDH), Calcium ( $\text{Ca}^{2+}$ ) levels and various hypoxia-responsive genes, induced during hypoxia stress. Abundance of *RBOHD* also changes under submergence due to oxidative stress (Yamauchi *et al.*, 2013, Yeung *et al.*, 2018). *SENESCENCE ASSOCIATED GENE (SAGs)* like *SAG12*, *SAG29*, and *ORESAR1 (ORE1/NAC6)* are mainly expressed in senescent tissue, which ultimately led to chlorophyll breakdown and leaf senescence. *SAG12* encodes a cysteine protease (vacuolar protein) in *Arabidopsis thaliana (Arabidopsis)* and is associated with oxidative stress ( $\text{H}_2\text{O}_2$ ) and senescence (Weaver *et al.*, 1998). Increased *SAG12* transcript leads to early leaf senescence in *Arabidopsis* (Ding *et al.*, 2016, Ueda *et al.*, 2020). Similarly, the *SAG29* gene is also prominently expressed in senescing plant tissues. The *SAG29* gene is highly induced by osmotic stresses through an abscisic acid-dependent pathway (Seo *et al.*, 2011). *ORE1* has been identified as an accession specific regulatory gene which is highly induced in Bay-0 ecotype (an *A. thaliana* accession) and has a predominant role in chlorophyll breakdown. The *ore1* mutant showed intermediary submergence tolerance (Yeung *et al.*, 2018). Both *ORE1* and *SAG29* accelerate leaf senescence in *Arabidopsis* (Kim *et al.*, 2009, Qiu *et al.*, 2015, Zhang *et al.*, 2018).

Besides genes and TFs, a large number of miRNAs have been also reported to be dynamically regulated under submergence stress (Zhang *et al.*, 2008, Moldovan *et al.*, 2010, Licausi *et al.*, 2011, Liu *et al.*, 2012, Jeong *et al.*, 2013, Zhai *et al.*, 2013, Jin *et al.*, 2017, Li *et al.*, 2017, Franke *et al.*, 2018, Fukao *et al.*, 2019). MicroRNAs belong to a class of endogenous small non-coding RNAs, which negatively regulate their target gene expression at the post-transcriptional level through complementary pairing with their specific target mRNAs in most of the eukaryotes. Several miRNAs have recently been implicated in various developmental processes, including

shoot and root development. Many miRNAs have been shown to be differentially expressed under various abiotic stress conditions (Singh *et al.*, 2020a, Wang *et al.*, 2020).

Previous reports showed the involvement of some miRNAs in the regulation of SAGs, such as miR164 mediated regulation of *ORE1* triggers early senescence by regulating various SAGs gene (Balazadeh *et al.*, 2010, Glazińska *et al.*, 2014, Yeung *et al.*, 2018). miR159 was found to be upregulated in maize root during waterlogging or flood conditions and its target Gibberellin Mediated expression of Myeloblastosis (*GAMYBs* such as, *MYB33* and *MYB101*) was downregulated (Liu *et al.*, 2012). miR166 is shown to have an important role in response to flood stress through regulating calcium spikes and accumulation of ROS during root growth and development (Fukao *et al.*, 2019). miR167 was found to regulate short-term waterlogging or submergence in maize root by targeting (*AUXIN RESPONSE FACTORS*) *ARFs* (Zhang *et al.*, 2008, Liu *et al.*, 2012). Recently, a report showed that miR167 was differentially upregulated in *Alternanthera philoxeroides* and *Populus tomentosa* plants during flood response (Li *et al.*, 2017). Moreover, miR156 have been indicated for its potential role in submergence and hypoxia by targeting *SQUAMOSA PROMOTER BINDING PROTEIN-LIKEs* (*SPLs*) genes in lotus and *Arabidopsis* (Moldovan *et al.*, 2010, Jin *et al.*, 2017, Franke *et al.*, 2018). Long-term waterlogging downregulated the expression of miR172 leading to accumulation of target *AP2/ERF* mRNAs and thereby promoted crown root development in maize (Zhai *et al.*, 2013). The expression of miR775, which targets *GALT9*, was reported to be induced by hypoxic condition caused by flood or high altitude in *Arabidopsis* (Moldovan *et al.*, 2010, Liu *et al.*, 2012, Jin *et al.*, 2017, Tripathi *et al.*, 2019). However, the functional role of miR775 in hypoxia remains to be understood. In the present study, we addressed the potential role of miR775-*GALT9* module in submergence stress induced hypoxia and post-submergence recovery in *A. thaliana*. Our study shows that miR775-*GALT9* module plays an important role in post-submergence recovery and senescence in *A. thaliana* by modulating the expression of SAGs, *RBOHD*, ethylene and ABA pathway genes.

## Results

### Gene structure of *MIR775A* and its possible origin through promoter acquisition

The *MIR775A* (AT1G78206) and its mature miR775, is uniquely present in *A. thaliana*, at chromosome 1 (Araport11; with gene coordinate Chr1:29422452-29422574). Interestingly, we did not find any promoter elements in the upstream (Transcription starts site (TSS) and TATA-box) of *MIR775A*. Hence, we searched for the existence of a canonical promoter element upstream to the *MIR775A* gene. We retrieved an intergenic sequence upstream of *MIR775A* to identify or predict the promoter through software ‘TSSPlant’ (<http://www.softberry.com/cgi-bin/programs/promoter/tssplant.pl>). We found an adjacent gene, *snoRNA* (AT1G09787.1), situated very closely (92 bp apart) in the upstream of *MIR775A*, having no predicted TSS or TATA-box (**Figure 1 a**). Therefore, we extended our search for the intergenic sequence between the next upstream genes AT1G78200 (in the upstream of *MIR775A*). We retrieved the intergenic sequence of 587 bp, including 3' UTR of AT1G78200 gene, which also included overlapping *snoRNA* sequence, and then predicted the TSS and TATA-box elements. (**Figure 1 a**). TSSPlant predicted two TSS- one was without TATA-Box and another with TATA-box (**Figure S1 a**). The predicted TSS with higher score (1.9844) also possessed a TATA-box and was considered as the best (**Figure S1 a**). This result suggests that *MIR775* putatively acquired the promoter elements to become functional, which is well fitted with earlier findings, stating promoter acquisition is also one of the modes of evolution of *MIRNAs* (Lu, 2019). However, we also checked other canonical modes of miRNA evolution to understand the origin of *MIR775* in *Arabidopsis*. To address this, we first investigated if *MIR775A* originated canonically through inverted duplication of its target (Allen *et al.*, 2004). We observed that *MIR775A* and its validated target *GALT9* genes are not situated in tandem, as they are 9.55 Mbp apart from each other in the chromosome 1 of *A. thaliana* genome (**Figure 1 b**), and possessed no duplicated fragment, ruling out its possible origin through inverted duplication mode, unlike common miRNAs. Further, we also checked the sequence variability at miR775 binding site in *GALT9* of *A. thaliana* against *GALT9* orthologs (**Figure S1 b**). However, we found a highly conserved miR775 binding site in *GALT9* orthologs (**Figure S1 b**), which also excludes the possibility of origin of *MIR775A* from *GALT9*. Therefore, our analysis indicates that the *MIR775A* possibly originated specifically in the genome of *A. thaliana* non-canonically through acquisition of TSS and TATA-box in its upstream region (**Figure 1 a**), which is a unique feature of miR775.

### Non-conserved miR775 targets conserved *GALT9*

During our ongoing work, other studies recently validated *GALT9* as a target of ath-miR775 in *A. thaliana* (Fahlgren *et al.*, 2007; Mishra *et al.*, 2021; Zhang *et al.*, 2021). Some more targets, *DCLI* (AT1G01040), *ATWRKY19* (AT4G12020) and *KFB* (*KELCH DOMAIN-CONTAINING F-BOX PROTEIN*, AT1G23390) were also predicted but not validated (Zhang *et al.*, 2011). *GALT9* got the status of bona fide target of miR775, surprisingly however, studies differed in terms of its cleavage site(s) (**Figure 1 c**). Our degradome analysis of the most recent TAIR database (AraPort11) using CleaveLand tool confirmed *GALT9* as the strongest target of miR775 in *A. thaliana*. Variable cumulative scores for a perfect cleavage site (10<sup>th</sup>) were obtained during degradome analysis in 11-day old seedling and leaf (**Figure 1 c, supplementary Table 1 and 2**). In seedling tissue, we observed the perfect cleavage site of miR775 in *GALT9* mRNA (position 10<sup>th</sup>), where all reads fell to CleaveLand analysis category (CAC) zero (0), the best score. However, in leaf, the miR775-mediated cleavage of *GALT9* appeared in CAC (2), suggesting moderate deviation from perfect cleavage site in some aligned reads (**Figure 1 c**). Thus, our results also indicate tissue specific variation of miR775 mediated cleavage of *GALT9* (**Figure 1 c, supplementary Table 1 and 2**). Thus, non-conserved miR775 is uniquely present specifically in *A. thaliana*, however, its target *GALT9* and *GALT9*-orthologues are widespread and conserved across the plant species (**Figure S1 b**).

### Expression pattern in co-infiltration experiment and mutant or transgenics showed negative regulation of *GALT9* by miR775

To further validate the transcriptional cleavage of *GALT9* by miR775, 4-week old *Nicotiana benthamiana* (Tobacco) leaves were co-infiltrated with construct 35S:*GALT9-GFP* (Control), Empty vector (EV)+35S:*GALT9-GFP*, and 35S:*MIR775A*+35S:*GALT9-GFP* (**Figure S2 a**). If cleaving *GALT9*, co-infiltrated miR775 should cleave the *GALT9* transcripts and reduce the expression of *GFP*. Parallely, we used another miRNA, miR839 as an additional control to validate that the *GALT9* is targeted by miR775 and co-infiltrated with 35S:*MIR839A*+35S:*GALT9-GFP*. Further, we quantified the level of *GFP* by quantitative RT-PCR (qRT-PCR) (**Figure S2 b**) and observed significant reduction in co-infiltrated (35S:*MIR775A* and 35S:*GALT9-GFP*) tobacco leaves in comparison to tobacco leaf co-infiltrated with 35S:*GALT9-GFP*, EV+35S:*GALT9-GFP*, and 35S:*MIR839A*+35S:*GALT9-GFP*.

Reduced expression of *GFP* confirmed the post-transcriptional cleavage of *GALT9* transcripts by miR775 (**Figure S2 b**). To further confirm the miR775 mediated downregulation of *GALT9* in *Arabidopsis*, we analyzed the expression of *GALT9* in two independent miR775 overexpression lines (miR775-Oe) (**Figure 2 a**) and observed its reduced expression (by 0.52 and 0.37 folds, respectively) (**Figure 2 b**). Further, we observed significant upregulation of *GALT9* transcript level in two independent lines having target mimic of miR775 (*MIM775-1* and *MIM775-2*), where miR775 activity is sponged, by 3.98 and 2.55-fold, respectively (**Figure 2 c**). These results confirmed the post-transcriptional regulation of *GALT9* by miR775, which is consistent with a recent study (Zhang *et al.*, 2021), published during the processing of this manuscript.

### Functional annotation by *GALT9* protein structure analysis

The 3D structure of *GALT9* was predicted using I-TASSER, which further deduces protein functions and biological annotations. We analyzed the enzyme commission (EC) numbers and gene ontology (GO) terms, and annotated their putative molecular function based on modelled 3D structure of *GALT9*. The best consensus putative function of *GALT9* has derived its role as an enzyme Beta-1,3-galactosyl-O-glycosyl-glycoprotein beta-1,6-N-acetylglucosaminyltransferase (EC number: 2.4.1.102) indicating its role in protein glycosylation (GO:0006486), where ligand is Uridine-Diphosphate (UDP) and involved in UDP-glycosyltransferase activity (GO:0008194) localized in Golgi membrane (GO:0000139) (**Figure S4 and S5**). These results indicate that *GALT9* involved in the transfer of glycosyl groups (GO:0016757) to protein moieties (e. g. the addition of glycan chains to proteins) through peptidyl-asparagine modification (GO:0018196). The peptidyl-asparagine modification helps in N-glycosylation, where glycans are attached to the side-chain nitrogen atoms of Asparagine (Asn) residues in a conserved consensus sequence Asparagine-Xaa-Serine/Threonine (Asn-Xaa-Ser/Thr), whereas Xaa might be any amino acid (Schwarz and Aebi, 2011).

### ***A. thaliana* GALT9 is a member of Carbohydrate Active enZyme (CAZy) family and the protein localizes in Golgi apparatus**

The coding sequence of *GALT9* consists of 1038 bp including seven exons which are interrupted by 6 introns while *GALT9* proteins consist of 345 amino acid residues (<https://www.arabidopsis.org/servlets/TairObject?name=AT1G53290&type=locus>). *GALT9* protein contains terminal glycosyl residue, which transfers to its substrate with help of UDP-galactose (Qu *et al.*, 2008, Gille *et al.*, 2013, Qin *et al.*, 2013). *GALT9* shows the strong homology with *Gossypium hirsutum* (cotton) *GhGALT1* and belongs to the Carbohydrate Active enZyme GlycosylTransferases (CAZy GT) family (Qin *et al.*, 2013). Total 31 members of the CAZy GT-family are present in *A. thaliana* and out of 31, 20 members have beta (1-3) GTs motif, similar to mammalian systems (Qu *et al.*, 2008). Since *GALT9* is potentially involved in post-translational modification of proteins, we investigated its subcellular localization. Using *Arabidopsis* “Subcellular Localization Prediction Server” (AtSubP, <http://bioinfo3.noble.org/AtSubP/index.php>). We predicted *GALT9* protein to be localized in Golgi apparatus, at subcellular level. To validate this, we generated a translation fusion reporter (*35S:GALT9-GFP*) construct and co-infiltrated it along with a Golgi apparatus marker (GmManI-pBIN2) mCherry for transient subcellular localization in *Nicotiana benthamiana* leaves. Using differential interference contrast (DIC) microscopic analysis, we found fluorescence from *35S:GALT9-GFP* to be primarily localised in the Golgi apparatus which is consistent with recently published by (Zhang *et al.*, 2021), further validating the *in silico* prediction (**Figure S5**).

### ***MIR775A* and target *GALT9* showed complementary and dynamic expression pattern predominantly in shoot and root tissues**

To investigate the spatiotemporal expression pattern of *MIR775A* and its target *GALT9*, we performed the histochemical GUS assay of 5 days after germination (dag) seedlings and 35 days old *pMIR775A:GUS* and *pGALT9:GUS* plants. In 5 dag seedlings, *MIR775A* showed expression in the shoot, hypocotyl, cotyledons, leaves, root shoot junction (RSJ), stomata, trichomes, and rosette leaves of 35 days old plants (**Figure 3 a-e**). *GALT9* is also expressed in shoot, root-shoot junction, hypocotyl, leaves, stomata, trichomes in 5 dag seedlings and rosette leaves of 35 days old plants (**Figure 3 f-j**). The GUS expression of *pMIR775A:GUS* and *pGALT9:GUS* was



complementary in shoot, shoot apex, root-shoot junction, hypocotyl, stomata, trichome, and rosette leaves.

Further, we quantified and compared the expression level among 5 dag whole seedlings, shoot and roots (**Figure 4 a**), which showed higher expression of *MIR775A* in shoot as compared to root (**Figure 4 a**). *MIR775A* and *GALT9* showed complementary expressions in cauline leaves, floral buds, and flower (**Figure 4 b**). The availability of mature miRNA depends on many factors like the activity of miRNA biosynthesis pathway genes, miRNA processing machinery, etc. (Chen, 2009). Therefore, we also validated the accumulation of functional mature miRNA in different tissues of 35 days old Col-0 plants by stem-loop qRT-PCR. The mature miR775 expressed abundantly in a young rosette, young cauline, floral bud, and flowers (**Figure 4 b**). These results suggest a dynamic spatiotemporal expression pattern of miR775 and its target *GALT9* in *A. thaliana*, which is likely to have an impact on its physiological or developmental role.

#### **Submergence stress affects the expression of miR775 and *GALT9* in *A. thaliana* seedlings**

Hypoxia stress condition, caused by flooding or high altitude, is known to induce the expression of miR775 in *Arabidopsis* (Moldovan *et al.*, 2010, Liu *et al.*, 2012, Jin *et al.*, 2017, Tripathi *et al.*, 2019). To understand the molecular basis of this, we first studied the effect of submergence induced hypoxia stress on the expression of miR775 and its target gene *GALT9* in *Arabidopsis* shoot. To analyse the submergence-induced expression of *MIR775A*, we have treated 7 dag seedlings under complete submergence and analyzed the expression of miR775 by stem-loop qRT-PCR and *GALT9* transcripts by qRT-PCR at four different time points (4hr, 8hr, 12hr, and 24hr) (**Figure 5 a**). We found the expression of miR775 was upregulated by 5 folds, however, the expression of its target *GALT9* was downregulated by 0.38 folds at 24 hr of submergence. However, the expression of miR775 was significantly upregulated at 4 hr but the expression of its target *GALT9* was not significantly changed. Further to analyse the tissue-specific expression, 7 dag shoot seedlings of *pMIR775A:GUS* and *pGALT9:GUS* transgenic plants were analyzed at two time points 4 hr and 24 hr during submergence stress (**Figure 5 b-g**). Interestingly, we found similar results to that of stem-loop qRT-PCR, under normoxic (normal level of oxygen) conditions, *pMIR775A:GUS* and *pGALT9:GUS* seedlings showed a basal level of expression in untreated seedlings (0 hr). At 4 hr after submergence, *Arabidopsis* seedlings resulted in mild

elevation of *pMIR775A:GUS* expression, however, at 24 hr after submergence, *pMIR775A:GUS* expression was upregulated (**Figure 5 b-d**) whereas expression of the *pGALT9:GUS* expression was significantly downregulated in shoot tissue (**Figure 5 g**). This result highlights the potential role of miR775 and its target *GALT9* during submergence stress in *Arabidopsis*.

### **Submergence recovery in miR775-Oe, MIM775, and *galt9* plants**

Complete submergence leads to the overproduction of different reactive oxygen species (ROS) due to the oxygen-deficient conditions (Bailey-Serres and Voesenek, 2008). Previously, we have shown that the expression of miR775 and *GALT9* was dynamically affected in a complementary way during submergence stress (**Figure 5**). Therefore, we were interested to estimate the survival ability in different miR775 transgenic lines and *galt9*. To estimate the survival rate, we have treated different transgenic lines before bolting of same stage (3-week-old) (miR775-Oe1, miR775-Oe2, *galt9*, and *MIM775-1*, *MIM775-2*) in complete submergence for 5 days and estimated their survival rate after 5 days of desubmergence (5DADS). We observed that nearly ~75% of the wild type (Col-0) plant survived during submergence recovery, however, the survivability rate was higher in miR775-Oe lines (~85-90%) and *galt9* (~90 %). The survival rate of *MIM775* was reduced to ~50%. (**Figure 6 m**). These results indicate that miR775 mediated regulation of its target gene *GALT9* contributes to the plant survival during post-submergence recovery.

### **Submergence stress altered the ROS levels in miR775-Oe, MIM775, and *galt9* plants**

To further understand the molecular function of miR775-*GALT9* module during submergence stress in *Arabidopsis*, we analyzed reactive oxygen species (ROS) accumulation. Hydrogen peroxide (H<sub>2</sub>O<sub>2</sub>) is one of the major ROS which accumulates during various abiotic and biotic stresses (Liu *et al.*, 2010). We have estimated the ROS (here H<sub>2</sub>O<sub>2</sub>) level in different miR775 transgenic lines (miR775-Oe and *MIM775*) and *galt9* mutant in 12 dag old seedlings after 5 dag of submergence through DAB staining. The accumulation of H<sub>2</sub>O<sub>2</sub> was highest in *MIM775-1* and *MIM775-2* (**Figure 7 a-f**). The level of H<sub>2</sub>O<sub>2</sub> reduced in miR775-Oe1, miR775-Oe2, and *galt9*, as compared to Col-0 control (**Figure 7a-f**). Further, we quantified the ROS intensity by using ImageJ (<https://imagej.nih.gov/ij/download.html>) (**Figure 7 g**). Next, we quantified the accumulation of *RBOHD*, a core hypoxia marker gene, after the 5 days of desubmergence and

we found increased expression of *RBOHD* in *MIM775* (2.19) as compared to miR775-Oe (0.01), *galt9* (0.03) lines (**Figure 7 h**). Increased expression of *RBOHD* in *MIM775* was persistent even after 5 days of desubmergence, suggesting ROS accumulation. This might have led to impaired growth during submergence due to the higher cell death. These higher levels of functional miR775, in miR775-Oe lines, promoted the plant survival ability during recovery from submergence stress, which might have reduced accumulation of ROS. Altered ROS levels in different miR775 transgenic and *galt9* lines suggest the differential ability of cells to survive.

### **Expression of SENESCENCE ASSOCIATED GENES (SAGs) and chlorophyll content were altered at post-submergence recovery**

Our results showed the poor recovery in *MIM775* lines after submergence in contrast to miR775-Oe and *galt9* lines (**Figure 6 m**). The *MIM775* transgenic lines have small rosette leaves, however, the miR775-Oe and *galt9* lines were phenotypically similar to the Col-0 control under normal growth and developmental conditions. *MIM775* transgenic lines exhibited enhanced senescence and a high degree of chlorosis after 5 days of post-submergence recovery (**Figure 6**). We observed reduction in senescence and chlorosis in miR775-Oe and *galt9* transgenic lines, as compared to *MIM775*. To further quantify chlorophyll breakdown, we estimated the level of Chlorophyll A, Chlorophyll B, total Chlorophyll, Carotenoids, and Xanthophylls at 5 days of desubmergence (**Figure 8 a-d**). We observed reduction in total chlorophyll level in *MIM775* transgenic lines, in contrast to miR775-Oe and *galt9* transgenic lines. The level of chlorophyll A, B, and xanthophyll was also reduced in *MIM775* lines (**Figure 8 a-d**).

An increase in ROS level and reduction in chlorophyll content after submergence stress is related to precocious senescence. Our results indicate that miR775-Oe and *galt9* plants survived through the submergence stress by reducing ROS level and chlorosis, and therefore, by delaying the senescence. On the other hand, the early senescence observed in *MIM775* plants (post-submergence) could be due to excessive ROS levels and reduced chlorophyll content (**Figure 7 a-f and g**) and (**Figure 8 a-d**).

Different abiotic and biotic stresses affect the expression of SAG genes like *SAG12*, *SAG29*, *ORE1* which further govern leaf senescence (Seo *et al.*, 2011, Yeung *et al.*, 2018, Bengoa Luoni *et al.*, 2019, Ueda *et al.*, 2020). We asked if miR775-*GALT9* mediated post-submergence recovery and senescence, as evidenced by phenotype in miR775 transgenic and *galt9* lines,

involved SAGs. To address that, we compared the expression level of *SAG12*, *SAG29*, and *ORE1* during post-submergence recovery. The expression level of *SAG12*, *SAG29*, and *ORE1* was downregulated in miR775-Oe1 and *galt9* transgenic lines whereas upregulated in *MIM775-1* (**Figure 8 e**). These data suggest that miR775-*GALT9* module regulates submergence tolerance and post-submergence recovery by modulating the expression of SAGs (*SAG12*, *SAG29*, and *ORE1*) in *A. thaliana*.

### **Putative molecular mechanisms and hormonal crosstalk during post-submergence recovery**

Phytohormones, such as ethylene (ET), abscisic acid (ABA) promotes leaf senescence (Wang *et al.*, 2021). In *Arabidopsis*, ethylene promotes leaf senescence through a signalling cascade mediated by *ETHYLENE INSENSITIVE 2 (EIN2)* - *EIN3*- *ORE1* (Kim *et al.*, 2009, Kim *et al.*, 2014). *EIN3*, a pivotal transcription factor (TF) of ET signalling directly activates the expression of *ORE1* and *SAG29* to promote leaf senescence (Kim *et al.*, 2014, Qiu *et al.*, 2015, Zhang *et al.*, 2018). To confirmed this further, we quantified the expression of *EIN2* and *EIN3* which acts upstream of *ORE1* and *SAG29* and we found *EIN2* and *EIN3* upregulated by 2.65 and 22.39-fold, respectively in *MIM775* (**Figure 8 f**) as compare to miR775-Oe1 and *galt9* (0.08 and 0.21-fold in miR775-Oe1, 0.45 and 0.34-fold in *galt9*, respectively). It has been reported that senescence associated NAC TFs such as *ANAC019*, *ANAC047*, *ANAC055*, *ORS1* and *ANAC102* and *ANAC087* acts downstream of *EIN2* and *EIN3* respectively to accelerate leaf senescence, chlorophyll breakdown and cell death which ultimately inhibit post submergence recovery (Kim *et al.*, 2014, Yeung *et al.*, 2018).

It has been shown previously in the current study that the expression of *RBOHD*, a core hypoxia marker gene was increased in *MIM775* (2.19) as compared to miR775-Oe (0.01), *galt9* (0.03) lines, after the 5 days of desubmergence (**Figure 7 h**). Increased expression of *RBOHD* in *MIM775* was persistent even after 5 days of desubmergence, suggesting ROS accumulation. It has been shown that osmotic stress causes oxidative stress led to oxidative cell damage and the ABA biosynthesis gene, *NINE-CIS-EPOXYCAROTENOID DIOXYGENASE 3 (NCED3)* was drastically upregulated by osmotic stress (Xiong *et al.*, 2002, Tamang and Fukao, 2015). Further, we quantified *NCED3* which has been shown to be upregulated by osmotic/oxidative stress and we found the expression of *NCED3* upregulated by 5.84-fold in *MIM775* (**Figure 8 f**) compare to miR775-Oe, and *galt9* (0.11 and 0.10). This increased *NCED3* leads to accumulation of ABA

and thus promotes stomatal closure which inhibits dehydration and ultimately affects post submergence recovery. These data suggest that miR775-*GALT9*-ET-ABA module regulates post-submergence recovery by modulating ethylene and abscisic acid signalling in *A. thaliana*.

## DISCUSSION

The miRNA-mediated gene regulation is crucial for the plant growth, development, and physiological responses, which facilitated the origin and evolution of miRNA through positive selection. Many of the miRNAs are evolutionarily categorized as ancient or young, based on their origin in plant species (Zhang *et al.*, 2006, Voinnet, 2009). Similarly, miR775 appears to be a young miRNA, which is called so due to its species-specific presence in *A. thaliana* (Lu *et al.*, 2006, Rajagopalan *et al.*, 2006). Earlier studies reported that plant species from *Poaceae* and *Brassicaceae* possessed many species-specific non-conserved miRNAs that originated through rapid spontaneous evolution (Zhang *et al.*, 2006, Cui *et al.*, 2017). Our study shows the *de novo* origin of *MIR775A* in *A. thaliana*. The genomic location of *MIR775A* and its validated target *GALT9*, and higher conservation of miR775-binding site at *GALT9* does not support the canonical modes of origin and evolution of miR775 (**Figure 1**). Further, we found its gene structure acquired through the acquisition of TSS and TATA-box in the upstream of two consecutive genes, *snoRNA* and *MIR775A* (**Figure 1a**, **Figure S1 a**). The continuous preferential selection pressure might be acted upon by the *A. thaliana* genome for the acquisition of promoter elements to regulate target gene *GALT9*. However, genetic drift, due to lack of selection, might have resulted in the loss of these genes in subsequent species divergence (Voinnet, 2009). Identification of miRNA, target genes, and their conservation across the species reveals the role of miRNA-target gene modulation in various aspects of plant growth and their physiology. The process like degradome PARE analysis often enables to identify conserved and novel targets. Our degradome analysis suggested *GALT9* as a strong target of miR775 in *A. thaliana* (**Figure 1 c**). In consistency with other observations, *GALT9* is validated and established as a bona fide target of miR775 (**Figure 1 c**) (Fahlgren *et al.*, 2007, Mishra *et al.*, 2021, Zhang *et al.*, 2021). Interestingly, however, variations in cleavage site of miR775 were obvious (**Figure 1c**), which might be depending upon the stage of growth, growth condition, and due to the biogenesis of miR775 from the 3' end of its stem-loop precursor (**Figure 1 b**). Additionally, in the present

study, we validated our *in silico* based prediction using I-TASSER and AtSubP shows that GALT9 protein localizes in the Golgi body (**Figure S4-S5**). The role of GALT9 was deduced from the predicted protein 3D structure through I-TASSER, which shows its protein glycosylation activity, as a part of post-translational modifications (PTM) required for folding and stabilizing the translated protein structures.

Environmental factors or abiotic stresses are known to influence the expression of many miRNAs, which are involved during the regulation of physiology as well as during growth and development of plants. It has been reported earlier that the hypoxic condition, caused by flood or high altitude leads, to the induction of miR775 indicating its potential role in hypoxia inducing stresses (Moldovan *et al.*, 2010, Liu *et al.*, 2012, Tripathi *et al.*, 2019).

Submergence severely affects plant growth and development, survivability, and yield by reducing light availability, stomatal opening, and thereby gaseous exchanges, which ultimately affects photosynthesis

and respiration. So, efficient recovery from the submergence stress is vital for plant growth and survival. In the current study, we showed the complementary regulation of miR775-*GALT9* module during the submergence stress-induced senescence and post-submergence recovery.

Our results have indicated the dynamic spatio-temporal expression pattern of miR775 and its target *GALT9* through reporter lines of *pMIR775A:GUS* and *pGALT9:GUS* under normal and submergence stress (**Figure 3 and 5**). Under normal conditions (without submergence), all the miR775 transgenic lines and *galt9* mutants were green and healthy, however, leaves of *MIM775* lines were small in size (**Figure 6 a-f**). Mutation in the light-response/signalling gene *HY5* is known to affect plant organ or leaf size (Zhang *et al.*, 2021). We showed that the expression of miR775 was increased in the shoot of *hy5-1* mutant (**Figure S6 b**). Further, HY5 protein is directly bound to the promoter of *MIR775*, as shown by the yeast-one-hybrid experiment (**Figure S6 a**). Therefore, HY5-mediated regulation of miR775 contributes to the altered leaf shape (organ size). These results implicate the role of HY5 in miR775-*GALT9* mediated organ size regulation (Zhang *et al.*, 2021). Many *GALT9* co-localized genes which encode Golgi body localized proteins (like *ACLA1*, *CGR2* and *CGR3* (**supplementary Table 4**) have been previously shown to play a key role in plant development such as *ATP-CITRATE LYASE A-1* (*acla1*) and *COTTON GOLGI-RELATED 2* (*cgr2-1*, *cgr3-1*) mutants have relatively smaller organ size (Fatland *et al.*, 2005, Kim *et al.*, 2015b).

We have characterized the miR775-*GALT9* module for its role in submergence stress recovery. Submergence stress causes reduction in oxygen level (hypoxia) (Nishiuchi *et al.*, 2012, Ahmed *et al.*, 2013, Chen *et al.*, 2015, Yeung *et al.*, 2018, Loreti and Striker, 2020, Nakamura and Noguchi, 2020). In our results, transgenics (miR775 overexpression, miR775-Oe1; and target mimic of miR775, *MIM775*), and obtained *galt9* mutant lines revealed significant differences in their submergence stress tolerance and post-submergence recovery. Among these miR775 transgenic and mutant lines, miR775-Oe1 and *galt9* exhibited the reduced accumulation of ROS (**Figure 7 a-f and g**). However, the *MIM775-1* line displayed an increased accumulation of ROS. It has been previously reported that after desubmergence, the reillumination conditions lead to the production of ROS in recovering tissues (Elstner and Osswald, 1994, Smirnov, 1995). ROS production was different between the miR775-Oe1, *galt9*, and *MIM775* lines, which corresponded to higher *RBOHD* accumulation during recovery in *MIM775*. *RBOHD*, a key hypoxia gene, and *RBOHD* mediated ROS burst is crucial for submergence tolerance and recovery (Yeung *et al.*, 2018). Balanced ROS production is crucial and needs to be countered by an effective antioxidant mechanism that can control excessive ROS production and associated damage in *Arabidopsis*. However, the recovery signals regulating *RBOHD* remain to be understood. A recent report shows that ABA and ethylene response in *Arabidopsis* is crucial for submergence tolerance and recovery (Yeung *et al.*, 2018). Increased cell death in *MIM775-1* during the submergence stress is also evident from the shoot after desubmergence (**Figure 7 a-f and g**). Upregulation of SAGs gene including *ORE1*, *SAG12*, and *SAG29* are marked during senescence (Weaver *et al.*, 1998, Seo *et al.*, 2011, Kim *et al.*, 2014, Qiu *et al.*, 2015, Ding *et al.*, 2016, Yeung *et al.*, 2018, Ueda *et al.*, 2020). Our result showed higher upregulation of *EIN2*, *EIN3*, *ORE1*, *SAG12*, and *SAG29* in *MIM775* lines, in comparison to miR775-Oe1, *galt9*, and Col-0 (**Figure 8 e**).

The miR775-Oe1 and *galt9* transgenics lines were healthy in comparison to Col-0 and *MIM775-1* at 5 days after desubmergence (**Figure 6 a-l**). *MIM775* lines were poorly affected by the submergence induced stress and showed early senescence during the submergence (**Figure 6 m**). (Qiu *et al.*, 2015, Yeung *et al.*, 2018). Submergence stress led to the yellowing of leaves in *MIM775-1* lines where chlorophyll content was least, in comparison to miR775-Oe1 and *galt9*, (**Figure 8 a-d**) suggesting that miR775- *GALT9* module regulate senescence and post submergence recovery (**Figure 8 a-d**).

Ethylene is known to be a senescence accelerating hormone and its signalling involve the *ETHYLENE- INSENSITIVE 2* (EIN2)–EIN3–NAC TFs to regulate leaf senescence and chlorophyll degradation. in *Arabidopsis* (Neljubow, 1901, Crocker, 1932, Kim *et al.*, 2015, Iqbal *et al.*, 2017). EIN3 directly activates the master regulator of SAG genes *ORE1* and *SAG29* to promote leaf senescence (Wang *et al.*, 2021).

EIN2 mediates leaf senescence by transducing ANAC019, ANAC047, ANAC055, and ORS1 TFs via EIN3 independent pathway. However, ANAC087 and ANAC102 TFs were preferentially activated by *ORE1* to promote leaf senescence, chlorophyll degradation and cell death (Kim *et al.*, 2014). Phytohormone ABA and ethylene regulate dehydration and senescence during submergence recovery by modulating SAG genes and *ORE1* (Yeung *et al.*, 2018). Enhanced expression of *RBOHD* promotes ROS accumulation which ultimately accelerates the expression of *NCED3* by oxidative stress (Xiong *et al.*, 2002). The ABA accumulation inhibits dehydration by stomatal closure and hampers post submergence recovery (Xiong *et al.*, 2002, Yeung *et al.*, 2018).

The role of GALT9 is deduced from the modelled protein structure through I-TASSER, which shows its protein glycosylation activity, which is a part of post translational modifications (PTM) required for folding and stabilizing the translated proteins such as many membrane proteins, secreted proteins and vacuolar proteins (Schwarz and Aebi, 2011, von Schaewen *et al.*, 2008). Earlier studies have shown that the hampered maturation of *N*-glycan in Golgi-complexes reduces the stress tolerance ability (Kang *et al.*, 2008, Nagashima *et al.*, 2018). Some of the proteins (EIN2, RBOHD etc.) involved in the post-submergence directed senescence network, were membrane bounded and acted as signal receptors. However, any perturbation in *N*-glycosylation disrupts the activity of membrane bounded signal receptors (Nagashima *et al.*, 2018). Further, we observed that *SAG12*, a senescence associated vacuolar protein, undergo *N*-glycosylation ([https://www.uniprot.org/uniprot/Q9FJ47#ptm\\_processing](https://www.uniprot.org/uniprot/Q9FJ47#ptm_processing)) might be processed by GALT9 (**Figure S4 and S5**). The connection between the miR775-GALT9 module and ethylene and ABA pathways is likely to be indirect. Since, GALT9 is not a transcription factor and likely to regulate the downstream genes through post-translational modification. *N*-linked glycosylation of phytohormonal pathway components (proteins) is crucial for hormonal homeostasis and required for physiological and developmental response (Jiao *et al.*, 2020, Li and Lan, 2017, Ostrowski and Jakubowska, 2014). Recently it has been predicted that ethylene biosynthetic



pathway gene such as S- adenosyl- l- methionine (SAM), ACC synthase (ACS), and ACC oxidase (ACO) proteins have N-linked glycosylation sites (Ahmadizadeh *et al.*, 2020). Ethylene is known to promote the accumulation of EIN2 and EIN3 (Qiao *et al.*, 2009), which showed enhanced expression in *MIM775* lines (**Figure 8 f**), which have higher GALT9 level. Therefore, we hypothesized that GALT9 mediated possible N-glycosylation of ethylene biosynthetic component (e.g., SAM, ACS and ACO) might have led to the altered accumulation of EIN2 and EIN3, which have affected post-submergence recovery in mutants/transgenics of miR775/GALT9 (**Figure 8 f and Figure 9**). On the other hand, the accumulation and homeostasis of endogenous ABA level is regulated by AtBG1 (an efficient  $\beta$ -glucosidase) which is involved in the hydrolysis of glucose-conjugated ABA (Jin *et al.*, 2011., Lee *et al.*, 2006). Since the glycoprotein AtBG1 possessed N-glycosylation sites, it is possible that GALT9 mediated glycosylation helps in the activation of AtBG1, which in turn hydrolyzes the conjugated form of ABA (Glucose-ABA) to produce active ABA. ABA increases the expression of NCED3 (an ABA biosynthetic gene) in a positive feedback mechanism (Barrero *et al.*, 2006). We showed the increased expression of NCED3 (an ABA biosynthetic gene) in *MIM775* lines during post submergence recovery, which might be due to GALT9 mediated glycosylation of AtBG1 (**Figure 8 f and Figure 9**).

In summary, we have illustrated the role of the miR775-*GALT9* module during submergence-induced recovery response. Our results suggest that miR775 promotes recovery after submergence by downregulating the expression of target *GALT9*. *GALT9* overexpression, caused in the *MIM775* line, led to the severe senescence of plants (**Figure 6**). miR775-*GALT9* module regulates the post-submergence recovery through the regulation of *EIN2*, *EIN3*, and SAGs either directly or indirectly. Increased expression of *EIN2*, *EIN3*, *NCED3*, and SAGs in the *MIM775* lines promotes cell death and chlorosis, which may be the consequence of increased ROS due to altered *GALT9* abundance and changes in the ethylene and ABA biosynthesis pathway genes (**Figure 8 e**). Based on our findings, we proposed the hypothetical model showing the importance of miR775-*GALT9* module in regulating the post-submergence recovery process in *A. thaliana* (**Figure 9**).

## Material and methods

### Evaluation and origin of *ath-miR775* in *Arabidopsis*

We evaluated the mode of origin of *miR775* in *Arabidopsis*. We calculated the distance between *MIR775A* (Chr1:29422452) and *GALT9* (Chr1:19873727) genes and found to be 9.55 Mbp apart on chromosome 1 (Araport11). Further, sequence alignment between *GALT9* and *MIR775A* did not show any duplication of *GALT9* in *MIR775A*. Consequently, we also searched for conservation or variation of complementary *miR775* binding sites in *GALT9* homologs through multiple sequence alignment using ClustalX (Larkin *et al.*, 2007). Multiple sequence alignment of top 19 hits of the *GALT9* homologs have shown conserved complementary *miR775* binding sites (**Figure S1 b**). Further, we predicted the promoter of *MIR775A* using the tool TSSPlant (<http://www.softberry.com/cgi-bin/programs/promoter/tssplant.pl>). In the upstream of *MIR775A*, we found gene *snoRNA* (AT1G09787.1) at a distance of 92bp, but no Transcription start site (TSS) and TATA box. Therefore, we took the upstream sequence extended from *MIR775A* to AT1G78200, and TSSPlant predicted TATA box and TSS at a distance of 387bp and 356bp, respectively upstream to *MIR775A*.

### Validation of *miR775* target using degradome data

We analyzed the target of *miR775* through the analysis of *Arabidopsis* degradome PARE data available at Sequence Read Archive (SRA) in NCBI (SRR3143654 – 11-day old seedling, SRR7093799 - leaf sample of stage 5) using tool CleaveLand v4.5 (used to find evidence/s of sliced targets of small RNAs from degradome data) (Addo-Quaye *et al.*, 2009) retrieved SRA datasets, SRR3143654 and SRR7093799, and then further converted into fastq and subsequently into fasta file formats using locally installed tools fastq-dump from SRA Toolkit (<https://www.ncbi.nlm.nih.gov/books/NBK158900/>) and FASTX-Toolkit ([http://hannonlab.cshl.edu/fastx\\_toolkit/](http://hannonlab.cshl.edu/fastx_toolkit/)), respectively. The tool fastx\_trimmer from FASTX-Toolkit was used for trimming the adapter sequences from these datasets. Further, the isoforms of mature *miR775* sequences were used as query against the whole genome cDNA sequences of *Arabidopsis* ([https://www.arabidopsis.org/download/index-auto.jsp?dir=%2Fdownload\\_files%2FSequences%2FAraport11\\_blastsets](https://www.arabidopsis.org/download/index-auto.jsp?dir=%2Fdownload_files%2FSequences%2FAraport11_blastsets)). The SRA datasets, mature *miR775* sequences and cDNA reference sequences of *Arabidopsis* were used for the analysis of *miR775* target through CleaveLand4 pipeline using default settings. The aligned reads of SRA datasets were considered

as a target which were being cut at 10th position in miR775. The miRNA-target cleavage site which has CleaveLand analysis category  $(0 - 4) \leq 2$ , lowest Allen et al. score  $(0 - \infty)$ , and highest MFE ratio  $(0 - 1)$  are considered as a best target.

### **Construction of transgenic lines**

For miR775 overexpression, the DNA fragments corresponding to the precursors of 238 bp were cloned, fused to the cauliflower mosaic virus 2X35S promoter gateway cloning vector pMDC32, and transformed into ecotype Columbia (Col-0). For the expression pattern of p*GALT9*:*GUS*, the 1256bp length of promoter sequence of *GALT9*, was cloned into pCAMBIA1301, fused to the glucuronidase (*GUS*) reporter gene as p*GALT9*:*GUS*, and transformed into Col-0 via *Agrobacterium*-mediated transformation. For localization and target validation, the full-length CDS of *GALT9*, 1038bp were cloned in the pCAMBIA1304 vector frame like 35S:*GALT9*:*GFP* by removing the stop codon. The target mimic line *MIM775* was generated by modifying the *IPSI* gene (Todesco *et al.*, 2010). *MIM775* target mimic constructs were placed in pGREEN vectors under constitutive CaMV 35S promoter which is resistant against BASTA. Col-0 ecotype was used as control throughout the experiment. Seeds of *galt9* (AT1G53290) SALK\_015338 were obtained from *Arabidopsis* Biological Resource Center (ABRC) (Ohio State University, Columbus, OH). The two independent lines showing the maximum upregulation of miR775, miR775-Oe1 (14.19-fold) and miR775-Oe2 (5.46-fold) were selected on Hygromycin B for further analysis in T3 generation. For miR775 mimic (*MIM775*) lines the two lines exhibiting the maximum upregulation of *GALT9* in *MIM775-1* (3.98-fold) and *MIM775-2* (2.55-fold) were selected on BASTA for the further analysis in T3 generation. Additionally, we generated *GALT9*-Oe1 (2.44-fold) and *GALT9*-Oe2 (3.04-fold) and were selected on Hygromycin B for further analysis in T3 generation. Primer details are provided in **supplementary table 3**.

### **Plant Growth and Submergence Treatment**

For all the experiments the *Arabidopsis* seeds were first sterilized by seed wash buffer (70% ethanol and 0.1% (v/v) Triton X-100) and then germinated on half-strength Murashige and Skoog ( $\frac{1}{2}$ MS) medium (HiMedia, Mumbai, India) supplemented with 1% sucrose and 0.8% agar (Murashige and Skoog, 1962). The plants were grown vertically in a controlled environment at

21-22°C, under the 16 hr light: 8 hr dark cycle of white light intensity at 120  $\mu\text{moles}/\text{m}^2/\text{s}$ . The above experiments were repeated in triplicates to ensure precision and reproducibility.

For submergence treatment, we used 3-week-old Col-0 plant, the disinfected tubs were filled with Milli-Q water overnight before the treatment to maintain temperature equilibrium (21-22°C) as previously described with some modifications and submerged (8hr after the start of the photoperiod) in ~6 cm water depth in a dark, humidity-controlled condition room (Yeung *et al.*, 2018). After 5 day of submergence, de-submerged plants were replaced under normal growth conditions for 5 days to follow the post submergence recovery. Submergence related experiments were performed at 2:00 PM (8hr after the start of the photoperiod).

### **Conditions for the Expression analysis of *MIR775A* and target *GALT9* during submergence stress in *A. thaliana* seedlings at different time points**

For submergence treatment, the disinfected tubs were filled with Milli-Q water overnight before the treatment to maintain the temperature equilibrium (21- 22°C). The 7 dag seedlings of *pMIR7775A: GUS*, *pGALT9:GUS*, and Col-0 plants contain half MS media in disposable, square plate Petri dishes (120x120x17) mm ht. (company Praveen Scientific Corporation) were used throughout the experiment. The plants were submerged (8h after the start of the photoperiod) at 2:00 PM in ~6 cm water depth in a dark, humidity-controlled condition room. The samples were harvested for GUS analysis at early and late time points of 4 hrs, and 24 hrs. For control plants, the samples were kept in dark for the same period without giving submergence to nullify the effect of the dark with submergence, and then samples were harvested for GUS analysis. For GUS analysis samples were incubated at 37°C for 14.5 hrs.

### ***Agrobacterium* infiltration with transgenic constructs validation of for miRNA target**

4-week-old *Nicotiana benthamiana* leaves were used for target validation. miR775-Oe and miR839-Oe cloned in pSITE-4NB vector and sensitive 35S:*GALT9:GFP* constructs were used to transform in *Agrobacterium tumefaciens* GV3101 strain. For infiltrations, the overnight cultures were harvested of individual construct and then suspended in an infiltration buffer (pH 5.7, 0.5% glucose 10 mM MgCl<sub>2</sub>, 150  $\mu\text{M}$  acetosyringone, and 10 mM MES,) and incubated at room temperature for 6 hrs. For target validation, *Nicotiana* leaves were infiltrated by 1 ml syringe with the target constructs (sensitive 35S:*GALT9:GFP*) alone or EV+35S:*GALT9:GFP*,

35S:*MIR775A*+35S:*GALT9:GFP*, and 35S:*MIR839A*+35S:*GALT9:GFP* in a 1:1 ratio of constructs. The plants were kept in a growth chamber maintained at 26 °C (+/-2) and light intensity of 250  $\mu\text{M}$  per  $\text{m}^2$  per s and harvested after 48 hrs for RNA extraction. For target validation, the *HPTII* gene in the vector was used to normalize target abundance in qRT-PCR experiments. For precursor efficiency in qRT-PCR assays, the Ct value of precursor expression was checked to confirm the synthesis of precursor miRNA in the overexpression construct.

### **Homology search for miR775 and target *GALT9***

We performed BLAST for the identification of precursor *MIR775A* and *GALT9* homologs in other plants. We did not find any homolog of miR775 in plants even by changing the search parameters of BLAST. However, *GALT9* shows homologs in other plants. A phylogenetic tree was reconstructed using the BLAST hits of *GALT9* through NCBI with the identity and query coverage (<https://blast.ncbi.nlm.nih.gov/Blast.cgi>).

### **3D structure prediction and analysis**

The functional annotation of *GALT9* protein was accomplished by analyzing its 3D structure. However, 3D solved structure of *GALT9* is not present in Protein Data Bank archive (PDB; <https://www.rcsb.org/>). Therefore, we used I-TASSER (Iterative Threading ASSEmbly Refinement), an online server (<https://zhanglab.dcmf.med.umich.edu/I-TASSER/>), for protein 3D structure prediction and structure-based function annotation, which uses a hierarchical and multiple threading approaches. The 3D structures of the best predicted model of *GALT9* were visualized through Chimera v1.6.2 (**Figure S3 a**). The stereochemical quality check through Ramachandran plot of the predicted *GALT9* structure confirmed its stable structure (**Figure S3 b**). Simultaneously, the functional annotation was also predicted based on assigned Enzyme Commission (EC) numbers, gene ontology (GO) terms, and ligand binding sites with binding affinity (Zhang, 2008, Roy *et al.*, 2010, Yang *et al.*, 2015).

### ***GALT9* protein and its subcellular localization in planta**

To explore subcellular localization of *GALT9* protein, we used an *Arabidopsis* Subcellular Localization Prediction Server (AtSubP, <http://bioinfo3.noble.org/AtSubP/index.php>). For the prediction of *GALT9* subcellular localization, the amino acid composition-based Support Vector

Machine (SVM) found that GALT9 is a Golgi apparatus protein. To validate the subcellular localization, the coding sequence of the *GALT9* gene (without the stop codon) was cloned into the pCAMBIA1304. The *35S:GALT9:GFP* construct was then transformed into *Agrobacterium tumefaciens* GV3101 strain. *Agrobacterium* containing the *35S:GALT9:GFP* or Golgi apparatus marker (GmManI-pBIN2) mCherry constructs were grown to saturation in Luria-Bertani (LB) medium. Cultures were centrifuged and resuspended in 10 mM MgCl<sub>2</sub>, 10 mM MES, and 150 mM acetosyringone and kept at room temperature for 2 h. The cultures were then diluted to 1 OD600 unit and co-infiltrated into the abaxial side of young tobacco (*Nicotiana benthamiana*) leaf epidermis (four-week-old seedlings grown at 22° C) using a 1 ml syringe without the needle. Transformed leaves were analyzed 72 h after infection of the lower epidermis. Subsequently, fluorescence microscopy was performed on a Nikon 80i as employed to record and process the digital images. At least three independently transformed leaves were analyzed.

### **Histochemical detection of GUS assay and microscopy**

Histochemical GUS analysis was carried out by putting the samples into appropriate amounts of GUS histochemical GUS buffer (50 mM sodium phosphate, pH 5.7, 50 mM EDTA, pH 8.0; 0.1% Triton X-100, 2mM potassium ferrocyanide, 2mM potassium ferricyanide and 1mM 5-Bromo-4-chloro-3-indolyl- $\beta$ -D-glucuronic acid (X-Gluc) and incubated at 37°C for 14.5 hrs. Stained samples were washed with a de-staining solution having ethanol: acetone: glycerol (3:1:1 v/v/v) to remove chlorophyll and then microscopy was performed after putting the samples in chloral hydrate (TCI Chemicals) for 1 hr on a Nikon80i and Olympus SZX16 as employed to record and process the digital images.

### **Total RNA Extraction and Quantitative Real-Time PCR**

Gene-specific primers were designed using IDT software Inc. (USA) and custom synthesized from Sigma Aldrich (Merk, India). The total RNA was extracted by using TRIzol (TRI reagent). Purified RNA used for single-stranded cDNA was synthesized from 2.5  $\mu$ g RNA using oligo (dT) primer by high-capacity cDNA reverse transcription Kit (Thermo Fisher Scientific, India). The RT reaction consisted of total RNA, 0.8  $\mu$ l of 100 mM dNTP mix, 2  $\mu$ l of 10X reaction buffer, 1  $\mu$ l of random hexamer primer, 1  $\mu$ l of oligodT, and 1  $\mu$ l of Revert aid RT enzyme in a final volume of 20  $\mu$ l. The reaction was carried out at 25°C (10 mins) / 37°C (2 hrs) followed by

denaturation at 85°C for 5 mins. For performing qRT-PCR, the cDNAs were diluted to 20 ng with sterile MQ water. For each tissue type, separate PCR amplification reactions were set up for detecting different genes. The qRT-PCR reaction was set up by mixing 5 µl of 2X Power Syber® Green PCR Master Mix (Applied Biosystems, USA), 0.5µl of 10 µM each of forward and reverse primers, 2µl (40 ng) of cDNA and sterile MQ water to adjust the reaction volume to 10µl. qRT-PCR was carried out in Applied Biosystems ViiA 7 Real-Time PCR System with PowerUp™ SYBR™ Green Master Mix (Applied Biosystems™ by Fisher Scientific). The relative transcript level was calculated by using the  $2^{-\Delta\Delta CT}$  method which was normalized to *ACTIN7* as previously described by (Wang *et al.*, 2014, Singh *et al.*, 2020b).

For stem-loop cDNA synthesis total of 200ng of purified RNA was taken then mix with 0.5 µl 10 mM dNTP and nuclease-free water, incubating the mixture at 65°C for 5 mins and put on ice for 2 mins, brief centrifugation, and add, 4 µl 5× buffer (250 mM Tris-HCl (pH 8.3), 250 mM KCl, 20 mM MgCl<sub>2</sub>, 50 mM DTT 2 µl 0.1 M DTT) 0.25 µl RiboLock RNase Inhibitor (20 units/µl) 0.25 µl RevertAid H Minus M-MuLV Reverse Transcriptase (200 units/µl), 1 µl Stem-loop primer (1 µM) mix gently and centrifuge to bring the solution to the bottom of the tube and cDNA synthesis was performed by previously described by (Varkonyi-Gasic *et al.*, 2007). The cDNA was diluted up to 2 times before performing the real-time PCR. Fold change was calculated using formula  $FC = 2^{-\Delta\Delta Ct}$  as previously described by (Singh *et al.*, 2017, Gautam *et al.*, 2020, Singh *et al.*, 2020b).

### **Histochemical detection of H<sub>2</sub>O<sub>2</sub>**

The H<sub>2</sub>O<sub>2</sub> staining agent, 3,3'diaminobenzidine (DAB) (SRL), was dissolved in H<sub>2</sub>O by adjusting the pH to 3.8 with KOH. Freshly prepared DAB solution was used to avoid auto-oxidation. The 7 dag old seedling were transferred for 5 days for submergence, after 5 days of submergence the seedling was exposed to 1 hour of normal condition and then transferred for treatment and were immersed and infiltrated under vacuum with 1.25 mg ml<sup>-1</sup> DAB staining solution for 15 mins and incubated at room temperature for 6 hrs. The Stained seedlings were then bleached out in ethanol: acetic acid: glycerol (3:1:1/ v/v/v) solution for 30 mins and then images were taken by an Olympus SZX16 microscope and ImageJ system software (<https://imagej.nih.gov/ij/download.html>) was used for the quantification of ROS intensity. The brown colour visualization of H<sub>2</sub>O<sub>2</sub> was due to DAB polymerization.

### **Chlorophylls and xanthophyll's estimation**

Chlorophyll and xanthophyll were extracted from 100 mg of rosettes leave with 96% (v/v) by DMSO dark incubated at 65 °C for 30 mins and cooled to room temperature for 15 mins (Hiscox and Israelstam, 1979, Richardson *et al.*, 2002). Measuring the absorbance at 470, 645, and 663 nm by calibrating to zero with pure DMSO and was measured with a spectrophotometer plate reader (Synergy HT Multi-Detection Microplate Reader, BioTek Instruments). Measurements were done in 2 biological replicates. Chlorophyll A and B concentrations were calculated by the following Arnon`s equations:

$$\text{Chlorophyll A (mg/g fresh weight)} = [(12.7 \times A_{663}) - (2.69 \times A_{645})] \times (V/1000 \times W)$$

$$\text{Chlorophyll B (mg/g fresh weight)} = [(22.9 \times A_{645}) - (4.68 \times A_{663})] \times (V/1000 \times W)$$

$$\text{Total Chlorophylls Content} = (2008 \times A_{645} + 802 \times A_{663}) \times (V/1000 \times W)$$

$$\text{Carotenoids + xanthophylls (mg/g fresh weight)} = (1000 \times A_{470} - 1.90\text{ChlA} - 63.14\text{ChlB}/214) \times (V/1000 \times W), \text{ where } V = \text{volume of extract (ml)}, W = \text{fresh weight of the sample (g)}.$$

### **Yeast one hybrid assays**

Yeast one-hybrid assays (Y1Hs) were performed to verify the gene-gene interactions, using the Matchmaker™ Gold Y1H Library Screening System. The full-length CDS of *HY5* was subcloned into the *GADT7* AD vector and the promoter of *pMIR775A* (~152 bp) was constructed into the public vector according to the ClonExpress II One-Step Cloning Kit. Auto-activation and then interaction analyses were performed.

### **Determination of autoactivation concentration of AbA**

A healthy colony was picked from the bait strains. The colony was resuspended in SD-Ura broth. The dilution was adjusted to 0.1, 0.01, 0.001, and 0.0001 and 10µl of the culture was patched on the following media: (i) SD/-Ura with AbA (150 ng/ml), (ii) SD/-Ura with AbA (250 ng/ml), (iii) SD/-Ura with AbA (500 ng/ml) and Vector/Construct details: (i) pGADT7 (for cloning of prey), (ii) pAbAi (for cloning of bait), (iii) pGADT7-Rec-p53/p53-AbAi (positive control), (iv) pGADT7 transformed in Y1H gold cells (negative control) and colonies were grown for 2–3 days at 28 °C on SD/-Ura plates.



## Statistical analysis

All data in this study were obtained from three independent experiments. Error bars indicate standard error ( $\pm$ SE). The data were analyzed with the two-tailed Student's t test using GraphPad Prism 9.0.0 software (<https://www.graphpad.com/quickcalcs/ttest1/?format=SEM>). Asterisks indicate significant statistical differences\*\*\*  $P \leq 0.001$ , \*\*  $P \leq 0.01$ , \*  $P \leq 0.05$  using t-test.

## Accession numbers

*Arabidopsis* Genome Initiative (AGI) locus identifiers for the genes mentioned in this article are listed as follows: *MIR775A* (AT1G78206), *GALT9* (AT1G53290), *SAG12* (AT5G45890), *SAG29* (AT5G13170), *ORE1* (AT5G39610), *RBOHBD* (AT5G47910), *HY5* (AT5G11260), *EIN2* (AT5G03280), *EIN3* (AT3G20770), and *NCED3* (AT3G14440).

## ACKNOWLEDGMENTS

We acknowledge NIPGR for providing necessary research facilities (plant growth facility, confocal/other microscopic facility, other central instrument facility) and internal grants. We acknowledge the Department of Biotechnology (DBT), Govt. of India for financial support (BT/PR12766/BPA/188/63/2015) and fellowship to VM (DBT/JRF/15/AL/223). We also acknowledge DBT-eLibrary Consortium (DeLCON) for providing access to e-resources. AKS acknowledges support from NIPGR and SLS, Jawaharlal Nehru University.

## AUTHOR CONTRIBUTIONS

VM performed and designed most of the experiments. ArS and VM prepared a manuscript draft and revised it. AK, NG, ArS, SSD, and SY contributed to some experiments and preparation of manuscript and its revision. AKS has conceptualized and supervised the work, interpreted data, revised the manuscript, and arranged funds.

## CONFLICT OF INTEREST

All authors declare no conflict of interest.

**DATA AVAILABILITY:** All data and materials will be made available to researchers upon request.

## LITERATURE CITED

- Addo-Quaye, C., Miller, W. and Axtell, M.J.** (2009) CleaveLand: a pipeline for using degradome data to find cleaved small RNA targets. *Bioinformatics (Oxford, England)*, **25**, 130-131.
- Ahmadzadeh, M., Chen, J.-T., Hasanzadeh, S., Ahmar, S., Heidari, P. J. J. o. G. E. and Biotechnology** (2020). Insights into the genes involved in the ethylene biosynthesis pathway in *Arabidopsis thaliana* and *Oryza sativa*. **18**, 1-20.
- Ahmed, F., Rafii, M.Y., Ismail, M.R., Juraimi, A.S., Rahim, H.A., Asfaliza, R. and Latif, M.A.** (2013) Waterlogging Tolerance of Crops: Breeding, Mechanism of Tolerance, Molecular Approaches, and Future Prospects. *BioMed Research International*, **2013**, 963525.
- Allen, E., Xie, Z., Gustafson, A.M., Sung, G.-H., Spatafora, J.W. and Carrington, J.C.J.N.g.** (2004) Evolution of microRNA genes by inverted duplication of target gene sequences in *Arabidopsis thaliana*. *Nature Genetics*, **36**, 1282-1290.
- Bailey-Serres, J. and Voeselek, L.A.** (2008) Flooding stress: acclimations and genetic diversity. *Annual review of plant biology*, **59**, 313-339.
- Balazadeh, S., Siddiqui, H., Allu, A.D., Matallana-Ramirez, L.P., Caldana, C., Mehrnia, M., Zanon, M.I., Köhler, B. and Mueller-Roeber, B.J.T.P.J.** (2010) A gene regulatory network controlled by the NAC transcription factor ANAC092/AtNAC2/ORE1 during salt-promoted senescence. *The Plant Journal*, **62**, 250-264.
- Barrero, J. M., Rodríguez, P. L., Quesada, V., Piqueras, P., Ponce, M. R., Micol, J. L. J. P., cell and environment** (2006). Both abscisic acid (ABA)-dependent and ABA-independent pathways govern the induction of NCED3, AAO3 and ABA1 in response to salt stress. **29**, 2000-2008.
- Bengoa Luoni, S., Astigueta, F.H., Nicosia, S., Moschen, S., Fernandez, P. and Heinz, R.** (2019) Transcription Factors Associated with Leaf Senescence in Crops. *Plants (Basel)*, **8**, 411.
- Bui, L.T., Shukla, V., Giorgi, F.M., Trivellini, A., Perata, P., Licausi, F. and Giuntoli, B.J.b.** (2020) Differential submergence tolerance between juvenile and adult *Arabidopsis* plants involves the ANAC017 transcription factor. *The Plant Journal*, Volume **104**, Issue **4**, 979-994
- Chen, L., Liao, B., Qi, H., Xie, L.-J., Huang, L., Tan, W.-J., Zhai, N., Yuan, L.-B., Zhou, Y., Yu, L.-J., Chen, Q.-F., Shu, W. and Xiao, S.** (2015) Autophagy contributes to regulation of the hypoxia response during submergence in *Arabidopsis thaliana*. *Autophagy*, **11**, 2233-2246.
- Crocker, W.J.P.o.t.A.P.S.** (1932) The effect of ethylene upon living organisms. *Proceedings of the American Philosophical Society*, **71**, 295-298.
- Cui, J., You, C. and Chen, X.** (2017) The evolution of microRNAs in plants. *Curr Opin Plant Biol*, **35**, 61-67.
- Ding, S., Wang, L., Yang, Z., Lu, Q., Wen, X. and Lu, C.J.J.o.i.p.b.** (2016) Decreased glutathione reductase2 leads to early leaf senescence in *Arabidopsis*. *J Integr Plant Biol*, **58**, 29-47.
- Eltner, E.F. and Osswald, W.J.P.o.t.R.S.o.E., Section B: Biological Sciences** (1994) Mechanisms of oxygen activation during plant stress. *Journal of Plant Physiology*, **102**, 131-154.
- Fahlgren, N., Howell, M.D., Kasschau, K.D., Chapman, E.J., Sullivan, C.M., Cumbie, J.S., Givan, S.A., Law, T.F., Grant, S.R. and Dangl, J.L.J.P.o.** (2007) High-throughput sequencing of *Arabidopsis* microRNAs: evidence for frequent birth and death of MIRNA genes. *PLoS ONE*, **2**, e219.
- Fatland, B.L., Nikolau, B.J. and Wurtele, E.S.J.T.P.C.** (2005) Reverse genetic characterization of cytosolic acetyl-CoA generation by ATP-citrate lyase in *Arabidopsis*. *Plant Cell*, **17**, 182-203.
- Franke, K.R., Schmidt, S.A., Park, S., Jeong, D.-H., Accerbi, M. and Green, P.J.J.B.g.** (2018) Analysis of Brachypodium miRNA targets: evidence for diverse control during stress and conservation in bioenergy crops. *BMC Genomics*, **19**, 547.
- Fukao, T., Barrera-Figueroa, B.E., Juntawong, P. and Peña-Castro, J.M.** (2019) Submergence and Waterlogging Stress in Plants: A Review Highlighting Research Opportunities and Understudied Aspects. *Front. Plant Sci.*, **10**.

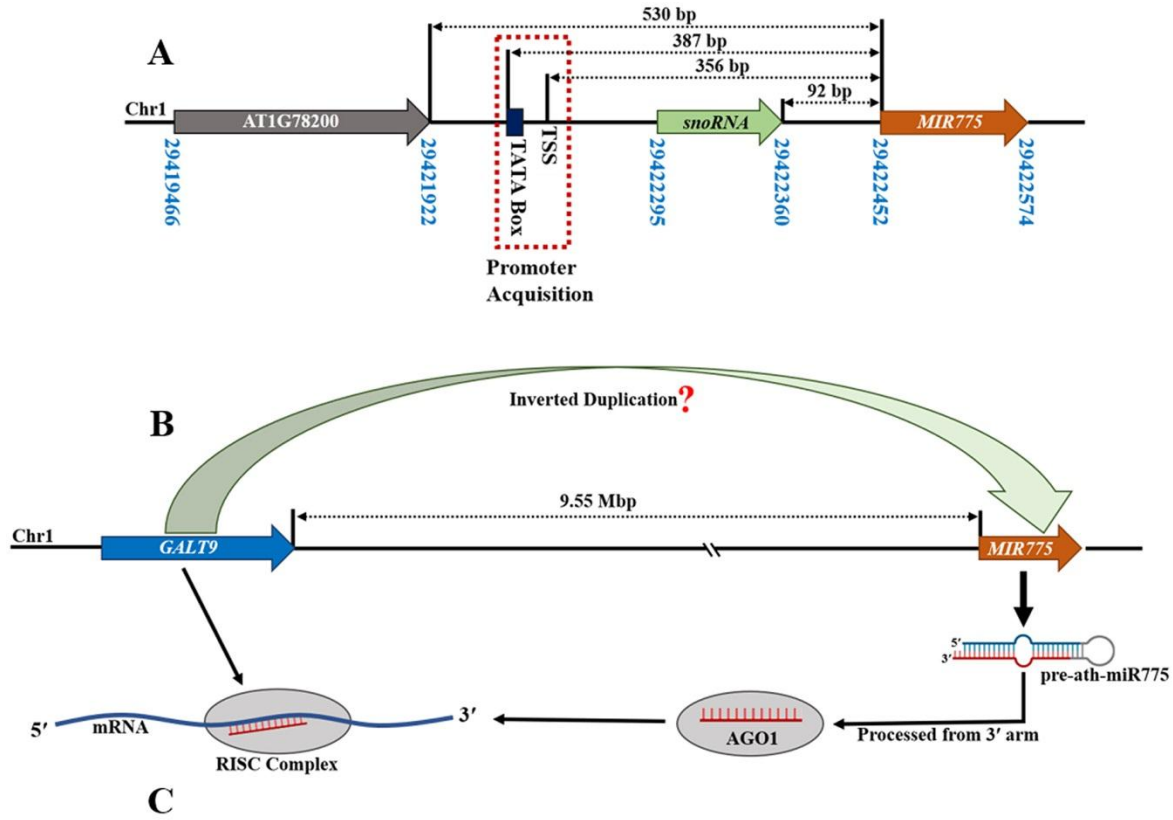
- Gautam, V., Singh, A., Yadav, S., Singh, S., Kumar, P., Das, S.S. and Sarkar, A.K.J.D.** (2020) Conserved LBL1-ta-siRNA and miR165/166-RLD1/2 modules regulate root development in maize. *Development*, **148**.
- Gille, S., Sharma, V., Baidoo, E., Keasling, J., Scheller, H. and Pauly, M.** (2013) Arabinosylation of a Yariv-Precipitable Cell Wall Polymer Impacts Plant Growth as Exemplified by the *Arabidopsis* Glycosyltransferase Mutant ray1. *Molecular plant*, **6**.
- Glazińska, P., Wilmowicz, E., Wojciechowski, W., Frankowski, K. and Kopcewicz, J.** (2014) Impact of InMIR319 and light on the expression of InTCP4 gene involved in the development of Ipomoea nil plants. *Acta Physiologiae Plantarum*, **36**, 29-43.
- Hiscox, J. and Israelstam, G.J.C.j.o.b.** (1979) A method for the extraction of chlorophyll from leaf tissue without maceration. *Canadian Journal of Botany*, **57**, 1332-1334.
- Iqbal, N., Khan, N.A., Ferrante, A., Trivellini, A., Francini, A. and Khan, M.J.F.i.p.s.** (2017) Ethylene role in plant growth, development and senescence: interaction with other phytohormones. *Front. Plant Sci.*, **8**, 475.
- Ismail, A.M.J.N.P.** (2018) Submergence tolerance in rice: resolving a pervasive quandary. *New Phytol.*, **218**, 1298-1300.
- Jeong, D.-H., Schmidt, S.A., Rymarquis, L.A., Park, S., Ganssmann, M., German, M.A., Accerbi, M., Zhai, J., Fahlgren, N. and Fox, S.E.J.G.b.** (2013) Parallel analysis of RNA ends enhances global investigation of microRNAs and target RNAs of Brachypodium distachyon. *Genome Biology*, **14**, R145.
- Jiao, Q., Chen, T., Niu, G., Zhang, H., Zhou, C. and Hong, Z. J. J. o. e. b.** (2020). N-glycosylation is involved in stomatal development by modulating the release of active abscisic acid and auxin in Arabidopsis. **71**, 5865-5879.
- Jin, Q., Xu, Y., Mattson, N., Li, X., Wang, B., Zhang, X., Jiang, H., Liu, X., Wang, Y. and Yao, D.J.F.i.p.s.** (2017) Identification of submergence-responsive microRNAs and their targets reveals complex miRNA-mediated regulatory networks in lotus (*Nelumbo nucifera* Gaertn). *Front. Plant Sci.*, **8**, 6.
- Jin, S., Kanagaraj, A., Verma, D., Lange, T. and Daniell, H. J. P. p.** (2011). Release of hormones from conjugates: chloroplast expression of  $\beta$ -glucosidase results in elevated phytohormone levels associated with significant increase in biomass and protection from aphids or whiteflies conferred by sucrose esters. **155**, 222-235.
- Kang, J.S., Frank, J., Kang, C.H., Kajiura, H., Vikram, M., Ueda, A., Kim, S., Bahk, J.D., Triplett, B. and Fujiyama, K.J.P.o.t.n.a.o.s.** (2008) Salt tolerance of *Arabidopsis thaliana* requires maturation of N-glycosylated proteins in the Golgi apparatus. *Proc Natl Acad Sci U S A*, **105**, 5933-5938.
- Kim, H.J., Hong, S.H., Kim, Y.W., Lee, I.H., Jun, J.H., Phee, B.-K., Rupak, T., Jeong, H., Lee, Y., Hong, B.S., Nam, H.G., Woo, H.R. and Lim, P.O.** (2014) Gene regulatory cascade of senescence-associated NAC transcription factors activated by ETHYLENE-INSENSITIVE2-mediated leaf senescence signalling in *Arabidopsis*. *J Exp Bot*, **65**, 4023-4036.
- Kim, J., Chang, C. and Tucker, M.L.** (2015a) To grow old: regulatory role of ethylene and jasmonic acid in senescence. *Front. Plant Sci.*, **6**.
- Kim, J.H., Woo, H.R., Kim, J., Lim, P.O., Lee, I.C., Choi, S.H., Hwang, D. and Nam, H.G.J.S.** (2009) Trifurcate feed-forward regulation of age-dependent cell death involving miR164 in *Arabidopsis*. *Science*, **323**, 1053-1057.
- Kim, S.J., Held, M.A., Zemelis, S., Wilkerson, C. and Brandizzi, F.J.T.P.J.** (2015b) CGR 2 and CGR 3 have critical overlapping roles in pectin methylesterification and plant growth in *Arabidopsis thaliana*. *The Plant journal*, **82**, 208-220.
- Kraehmer, H.** (2016) Morphological adaptation to water, pp. 192-193.
- Kumar, A. and Dash, P.K.** (2019) Transcriptome Analysis for Abiotic Stresses in Rice (*Oryza sativa* L.). In *Transcriptome Analysis*: IntechOpen.

- Larkin, M.A., Blackshields, G., Brown, N.P., Chenna, R., McGettigan, P.A., McWilliam, H., Valentin, F., Wallace, I.M., Wilm, A., Lopez, R., Thompson, J.D., Gibson, T.J. and Higgins, D.G. (2007) Clustal W and Clustal X version 2.0. *Bioinformatics*, **23**, 2947-2948.
- Lee, K. H., Piao, H. L., Kim, H.-Y., Choi, S. M., Jiang, F., Hartung, W., Hwang, I., Kwak, J. M., Lee, I.-J. and Hwang, I. J. C. (2006). Activation of glucosidase via stress-induced polymerization rapidly increases active pools of abscisic acid. **126**, 1109-1120.
- Li, G., Deng, Y., Geng, Y., Zhou, C., Wang, Y., Zhang, W., Song, Z., Gao, L. and Yang, J.J.F.i.p.s. (2017) Differentially expressed microRNAs and target genes associated with plastic internode elongation in *Alternanthera philoxeroides* in contrasting hydrological habitats. *Front. Plant Sci.*, **8**, 2078.
- Li, W. and Lan, P. (2017). The Understanding of the Plant Iron Deficiency Responses in Strategy I Plants and the Role of Ethylene in This Process by Omic Approaches. *Frontiers in Plant Science* **8**.
- Licausi, F., Weits, D.A., Pant, B.D., Scheible, W.R., Geigenberger, P. and van Dongen, J.T.J.N.p. (2011) Hypoxia responsive gene expression is mediated by various subsets of transcription factors and miRNAs that are determined by the actual oxygen availability. *Front. Plant Sci.*, **190**, 442-456.
- Liu, Z.-J., Guo, Y.-K. and Bai, J.-G.J.J.o.p.g.r. (2010) Exogenous hydrogen peroxide changes antioxidant enzyme activity and protects ultrastructure in leaves of two cucumber ecotypes under osmotic stress. *Journal of Plant Growth Regulation*, **29**, 171-183.
- Liu, Z., Kumari, S., Zhang, L., Zheng, Y. and Ware, D. (2012) Characterization of miRNAs in response to short-term waterlogging in three inbred lines of *Zea mays*. *PLoS One*, **7**, e39786-e39786.
- Loreti, E. and Striker, G.G. (2020) Plant Responses to Hypoxia: Signaling and Adaptation: Multidisciplinary Digital Publishing Institute. *Plants (Basel)*, **9**, 1704
- Lu, C., Kulkarni, K., Souret, F.F., MuthuValliappan, R., Tej, S.S., Poethig, R.S., Henderson, I.R., Jacobsen, S.E., Wang, W., Green, P.J. and Meyers, B.C. (2006) MicroRNAs and other small RNAs enriched in the *Arabidopsis* RNA-dependent RNA polymerase-2 mutant. *Genome research*, **16**, 1276-1288.
- Lu, S. (2019) De novo origination of MIRNAs through generation of short inverted repeats in target genes. *RNA Biology*, **16**, 846-859.
- Mishra, P., Singh, A., Verma, A.K., Singh, R. and Roy, S.J.b. (2021) microRNA775 targets a  $\beta$ -(1, 3)-galactosyltransferase to regulate growth and development in *Arabidopsis thaliana*. *bioRxiv.org*.
- Moldovan, D., Spriggs, A., Yang, J., Pogson, B.J., Dennis, E.S. and Wilson, I.W. (2010) Hypoxia-responsive microRNAs and trans-acting small interfering RNAs in *Arabidopsis*. *J Exp Bot*, **61**, 165-177.
- Murashige, T. and Skoog, F.J.P.p. (1962) A revised medium for rapid growth and bio assays with tobacco tissue cultures. *Physiologia plantarum*, **15**, 473-497.
- Nagashima, Y., von Schaewen, A. and Koiwa, H.J.P.S. (2018) Function of N-glycosylation in plants. *Plant Science*, **274**, 70-79.
- Nakamura, M. and Noguchi, K.J.J.o.P.R. (2020) Tolerant mechanisms to O<sub>2</sub> deficiency under submergence conditions in plants. *J Plant Res.*, **1-29**, 133:343–371
- Neljubow, D.J.B.C.B. (1901) Über die horizontale Nutation der Stengel von *Pisum Sativum* und einiger anderen Pflanzen. *Bot. Centralbl. Beih.*, **10**, 128-139.
- Nishiuchi, S., Yamauchi, T., Takahashi, H., Kotula, L. and Nakazono, M. (2012) Mechanisms for coping with submergence and waterlogging in rice. *Rice*, **5**, 2.
- Ostrowski, M. and Jakubowska, A. J. A. C. B. (2014). UDP-glycosyltransferases of plant hormones. **4**, 43-60.
- Pattyn, J., Vaughan-Hirsch, J. and Van de Poel, B. J. N. P. (2021). The regulation of ethylene biosynthesis: A complex multilevel control circuitry. **229**, 770-782.

- Qiao, H., Chang, K. N., Yazaki, J., Ecker, J. R. J. G. and development** (2009). Interplay between ethylene, ETP1/ETP2 F-box proteins, and degradation of EIN2 triggers ethylene responses in *Arabidopsis*. **23**, 512-521.
- Qin, L.-X., Rao, Y., Li, L., Huang, J.-F., Xu, W.-L. and Li, X.-B.J.P.O.** (2013) Cotton GalT1 encoding a putative glycosyltransferase is involved in regulation of cell wall pectin biosynthesis during plant development. *PLoS ONE*, **8**, e59115.
- Qiu, K., Li, Z., Yang, Z., Chen, J., Wu, S., Zhu, X., Gao, S., Gao, J., Ren, G. and Kuai, B.J.P.G.** (2015) EIN3 and ORE1 accelerate degreening during ethylene-mediated leaf senescence by directly activating chlorophyll catabolic genes in *Arabidopsis*. *PLoS Genet.*, **11**, e1005399.
- Qu, G., Kruszka, K., Plewka, P., Yang, S.-Y., Chiou, T.-J., Jarmolowski, A., Szweykowska-Kulinska, Z., Echeverria, M. and Karlowski, W. M.** (2015). Promoter-based identification of novel non-coding RNAs reveals the presence of dicistronic snoRNA-miRNA genes in *Arabidopsis thaliana*. *BMC Genomics* **16**, 1009-1009.
- Qu, Y., Egelund, J., Gilson, P.R., Houghton, F., Gleeson, P.A., Schultz, C.J. and Bacic, A.J.P.m.b.** (2008) Identification of a novel group of putative *Arabidopsis thaliana*  $\beta$ -(1, 3)-galactosyltransferases *Plant Molecular Biology*, **68**, 43-59.
- Rajagopalan, R., Vaucheret, H., Trejo, J., Bartel, D.P.J.G. and development** (2006) A diverse and evolutionarily fluid set of microRNAs in *Arabidopsis thaliana*. *Genes Dev.*, **20**, 3407-3425.
- Richardson, A.D., Duigan, S.P. and Berlyn, G.P.J.N.p.** (2002) An evaluation of noninvasive methods to estimate foliar chlorophyll content. *New Phytologist*, **153**, 185-194.
- Roy, A., Kucukural, A. and Zhang, Y.J.N.p.** (2010) I-TASSER: a unified platform for automated protein structure and function prediction. *Nature Protocols*, **5**, 725-738.
- Seo, P.J., Park, J.-M., Kang, S.K., Kim, S.-G. and Park, C.-M.J.P.** (2011) An *Arabidopsis* senescence-associated protein SAG29 regulates cell viability under high salinity. *Planta*, **233**, 189-200.
- Singh, A., Gandhi, N., Mishra, V., Yadav, S., Rai, V. and Sarkar, A.K.** (2020a) Role of abiotic stress responsive miRNAs in *Arabidopsis* root development. *Journal of Plant Biochemistry and Biotechnology*, **29**, 733-742.
- Singh, S., Singh, A., Yadav, S., Gautam, V., Singh, A. and Sarkar, A.K.** (2017) Sirtinol, a Sir2 protein inhibitor, affects stem cell maintenance and root development in *Arabidopsis thaliana* by modulating auxin-cytokinin signaling components. *Sci Rep*, **7**, 42450.
- Singh, S., Yadav, S., Singh, A., Mahima, M., Singh, A., Gautam, V. and Sarkar, A.K.** (2020b) Auxin signaling modulates LATERAL ROOT PRIMORDIUM1 (LRP1) expression during lateral root development in *Arabidopsis*. *The Plant journal*, **101**, 87-100.
- Smirnov, N.** (1995) *Environment and plant metabolism: flexibility and acclimation*: BIOS Scientific publishers.
- Tamang, B.G. and Fukao, T.** (2015) Plant Adaptation to Multiple Stresses during Submergence and Following Desubmergence. *Int J Mol Sci.*, **16**, 30164-30180.
- Todesco, M., Rubio-Somoza, I., Paz-Ares, J. and Weigel, D.** (2010) A collection of target mimics for comprehensive analysis of microRNA function in *Arabidopsis thaliana*. *PLoS genetics*, **6**, e1001031-e1001031.
- Tripathi, A.M., Singh, A., Singh, R., Verma, A.K. and Roy, S.** (2019) Modulation of miRNA expression in natural populations of *A. thaliana* along a wide altitudinal gradient of Indian Himalayas. *Sci Rep*, **9**, 441
- Ueda, H., Ito, T., Inoue, R., Masuda, Y., Nagashima, Y., Kozuka, T. and Kusaba, M.J.F.i.P.S.** (2020) Genetic Interaction Among Phytochrome, Ethylene and Abscisic Acid Signaling During Dark-Induced Senescence in *Arabidopsis thaliana*. *Front. Plant Sci.*, **11**.
- Varkonyi-Gasic, E., Wu, R., Wood, M., Walton, E.F. and Hellens, R.P.** (2007) Protocol: a highly sensitive RT-PCR method for detection and quantification of microRNAs. *Plant Methods*, **3**, 12.

- Visser, E., Voeselek, L., Vartapetian, B. and Jackson, M.J.A.o.B. (2003) Flooding and plant growth. *Ann Bot.*, **91**, 107-109.
- Voinnet, O.J.C. (2009) Origin, biogenesis, and activity of plant microRNAs. *Cell.*, **136**, 669-687.
- von Schaewen, A., Frank, J., Koiwa, H.J.P.s. and behavior (2008) Role of complex N-glycans in plant stress tolerance. *Plant Signal Behav.*, **3**, 871-873.
- Wang, C., Dai, S., Zhang, Z.L., Lao, W., Wang, R., Meng, X. and Zhou, X. (2021) Ethylene and salicylic acid synergistically accelerate leaf senescence in *Arabidopsis*. *Journal of integrative plant biology*, **63**, 828-833.
- Wang, H., Wang, J., Jiang, J., Chen, S., Guan, Z., Liao, Y. and Chen, F. (2014) Reference genes for normalizing transcription in diploid and tetraploid *Arabidopsis*. *Sci Rep*, **4**, 6781.
- Wang, Z., Feng, Y., Li, J., Zou, J., Fan, L.J.C.B., Genomics, P.P.D. and Proteomics (2020) Integrative microRNA and mRNA analysis reveals regulation of ER stress in the Pacific white shrimp *Litopenaeus vannamei* under acute cold stress. *Comparative Biochemistry and Physiology Part D: Genomics and Proteomics*, **33**, 100645.
- Weaver, L.M., Gan, S., Quirino, B. and Amasino, R.M.J.P.m.b. (1998) A comparison of the expression patterns of several senescence-associated genes in response to stress and hormone treatment. *Plant Molecular Biology*, **37**, 455-469.
- Xiong, L., Lee, H., Ishitani, M. and Zhu, J.-K.J.J.o.B.C. (2002) Regulation of osmotic stress-responsive gene expression by the *thel6/aba1* locus in *Arabidopsis*. *J Biol Chem.*, **277**, 8588-8596.
- Yamauchi, T., Shimamura, S., Nakazono, M. and Mochizuki, T. (2013) Aerenchyma formation in crop species: A review. *Field Crops Research*, **152**, 8-16.
- Yang, J., Yan, R., Roy, A., Xu, D., Poisson, J. and Zhang, Y.J.N.m. (2015) The I-TASSER Suite: protein structure and function prediction. *Nature Methods*, **12**, 7-8.
- Yeung, E., van Veen, H., Vashisht, D., Sobral Paiva, A.L., Hummel, M., Rankenberg, T., Steffens, B., Steffen-Heins, A., Sauter, M., de Vries, M., Schuurink, R.C., Bazin, J., Bailey-Serres, J., Voeselek, L.A.C.J. and Sasidharan, R. (2018) A stress recovery signaling network for enhanced flooding tolerance in *Arabidopsis thaliana*. *Proc Natl Acad Sci U S A*, **115**, E6085-E6094.
- Zhai, L., Liu, Z., Zou, X., Jiang, Y., Qiu, F., Zheng, Y. and Zhang, Z.J.P.p. (2013) Genome-wide identification and analysis of microRNA responding to long-term waterlogging in crown roots of maize seedlings. *Physiol Plant.*, **147**, 181-193.
- Zhang, B., Pan, X., Cannon, C.H., Cobb, G.P. and Anderson, T.A.J.T.P.J. (2006) Conservation and divergence of plant microRNA genes. *The Plant Journal*, **46**, 243-259.
- Zhang, C., Teng, X.D., Zheng, Q.Q., Zhao, Y.Y., Lu, J.Y., Wang, Y., Guo, H. and Yang, Z.N. (2018) Ethylene signaling is critical for synergid cell functional specification and pollen tube attraction. *The Plant journal*, **96**, 176-187.
- Zhang, H., Guo, Z., Zhuang, Y., Suo, Y., Du, J., Gao, Z., Pan, J., Li, L., Wang, T. and Xiao, L.J.T.P.C. (2021) MicroRNA775 Regulates Intrinsic Leaf Size and Reduces Cell Wall Pectin Levels by Targeting a Galactosyltransferase Gene in *Arabidopsis*. *Plant Cell*, **33** (3):581-602.
- Zhang, H., He, H., Wang, X., Wang, X., Yang, X., Li, L. and Deng, X.W. (2011) Genome-wide mapping of the HY5-mediated gene networks in *Arabidopsis* that involve both transcriptional and post-transcriptional regulation. *The Plant journal*, **65**, 346-358.
- Zhang, J., Van Toai, T., Huynh, L. and Preiszner, J.J.M.B. (2000) Development of flooding-tolerant *Arabidopsis thaliana* by autoregulated cytokinin production. *Molecular Breeding volume*, **6**, 135-144.
- Zhang, Y.J.B.b. (2008) I-TASSER server for protein 3D structure prediction. *BMC Bioinformatics*, **9**, 1-8.
- Zhang, Z., Wei, L., Zou, X., Tao, Y., Liu, Z. and Zheng, Y.J.A.o.b. (2008) Submergence-responsive microRNAs are potentially involved in the regulation of morphological and metabolic adaptations in maize root cells. *Ann Bot.*, **102**, 509-519.

# Figures



ath-miR775 and its target binding site		Cleavage site	Type of Analysis	Reference
<i>GALT9</i>	5' UCGUACUGCUAGAUUCGAA 3'	10 <sup>th</sup> – 12 <sup>#</sup> /0*	Degradome	Present study
Ath-miR775	3' ACCGUGACGAUCUGUAGCUU 5'	10 <sup>th</sup> – 5 <sup>#</sup> /2*		
Ath-miR775	ACCGUGACGAUCUGUAGCUU-5'	14 <sup>th</sup> – 5/20	5' RLM-RACE	Zhang et. al., 2021
<i>GALT9</i>	5' -UUCGUACUGCUAGAUUCGAA	15 <sup>th</sup> – 9/20		
<i>GALT9</i>	5' UCGUACUGCUAGAUUCGAA 3'	10 <sup>th</sup> – 9/12	5' RLM-RACE	Mishra et. al., 2021
Ath-miR775	3' ACCGUGACGAUCUGUAGCUU 5'			
<i>GALT9</i>	5' CUUCGUACUGCUAGAUUCGAA 3'	10 <sup>th</sup> – 1/21	5' RLM-RACE	Fahlgren et. al., 2007
Ath-miR775	3' ACCGUGACGAUCUGUAGCUU 5'			

\*Number of Reads; \*Cleaveland analysis category, lowest value is better

**Figure 1.** (a) Gene structure of *MIR775A* in *A. thaliana*, where the presence of predicted TSS and TATA-Box shows putative promoter (acquisition) in the upstream region. Numbers in blue color represents gene coordinates at chromosome 1, (b) putative mode of origin and processing of mature miR775, (c) comparative studies showing the variation of miR775 target cleavage sites in *GALT9* transcripts in *A. thaliana*. # Represents the number of reads in the degradome dataset cleaved at 10<sup>th</sup> position of miR775.



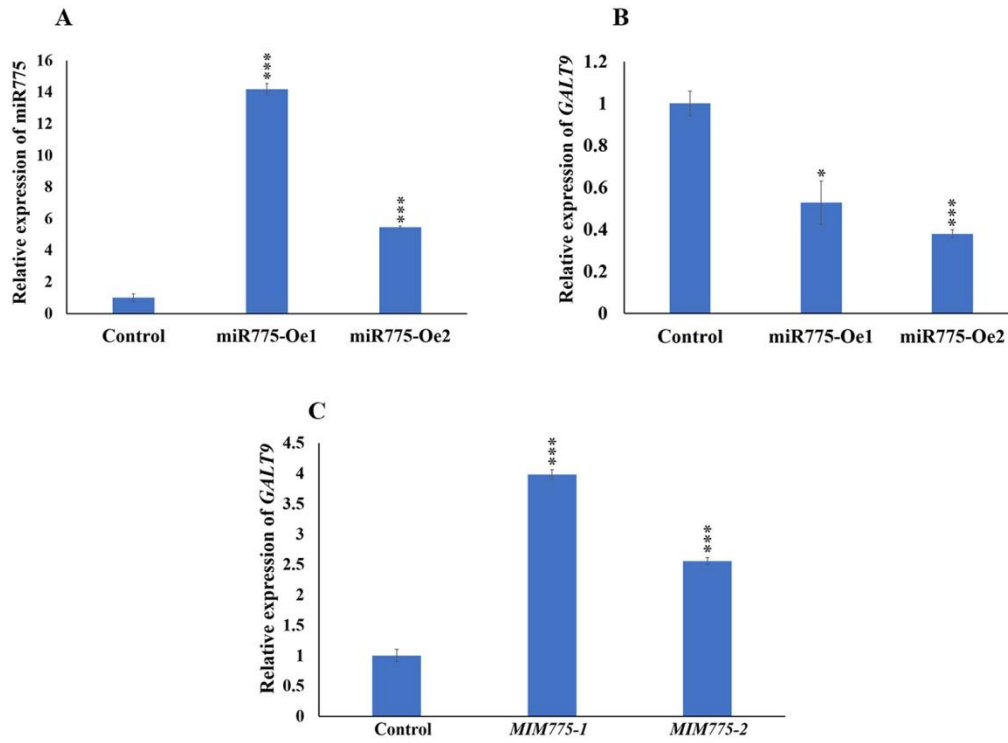


**Figure 2.** Relative expression of miRNA and their target *GALT9*. (a) relative quantification of miR775 expression in miR775-Oe1 and miR775-Oe2, (b) relative expression of *GALT9* in miR775-Oe1 and miR775-Oe2, (c) relative expression of *GALT9* in *MIM775-1* and *MIM775-2*. Error bars indicate standard error ( $\pm$ SE) of three independent experiments. Asterisks indicate significant statistical differences \*\*\*  $P \leq 0.001$ , \*\*  $P \leq 0.01$ , \*  $P \leq 0.05$  using t-test.

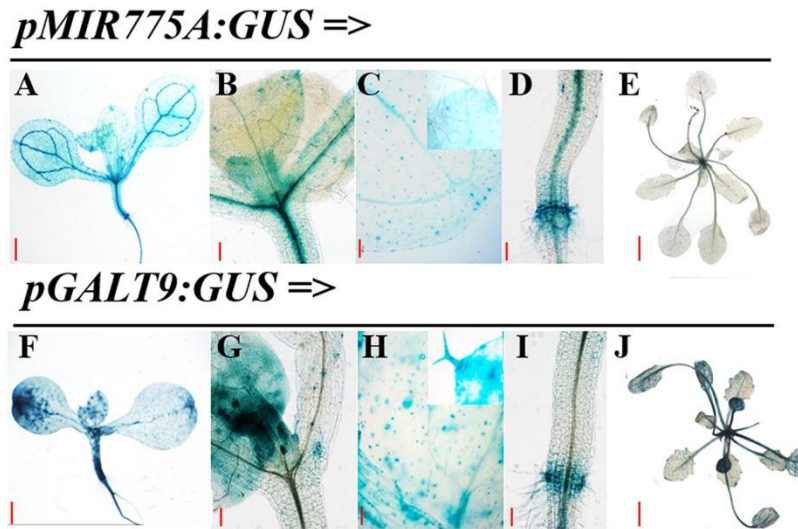


**Figure 3.** Tissue specific expression pattern of *MIR775A* and its target *GALT9* in *Arabidopsis thaliana*. (a-e) GUS expression of *MIR775A* in seedlings of 5 days after germination (dag), representation of expressions in different tissues are as following (a) shoot, (b) shoot apex, (c) cotyledon leaf, (d) root & shoot junction, (e) 35 dag rosette leaf. (f-j) showing GUS expression of target *GALT9* in (f) shoot, (g) shoot apex, (h) cotyledon leaf, (i) root & shoot junction, (e) 35 dag rosette leaf. n=15. Scale bar (red) = 100  $\mu$ m.

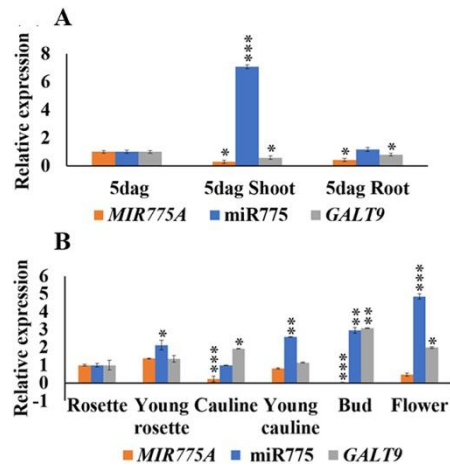


**Figure 4.** Relative expression of *MIR775A*, *miR775* and *GALT9* in various tissues of *A. thaliana*. (a) 5 dag seedlings and (b) 35 dag of plant. Error bars indicate standard error ( $\pm$ SE) of three independent experiments. Asterisks indicate significant statistical differences \*\*\*  $P \leq 0.001$ , \*\*  $P \leq 0.01$ , \*  $P \leq 0.05$  using t-test.

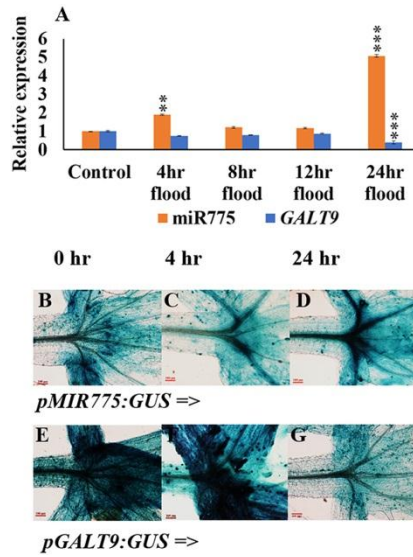


**Figure 5.** Expression pattern of *MIR775A* and target *GALT9* during submergence stress in *A. thaliana* seedlings at different time points. **(a)** relative expression level of miR775 and *GALT9* during submergence stress at different time points, **(b-d)** tissue specific expression of *pMIR775A:GUS*, **(b)** control (0 hr), **(c)** 4 hr, **(d)** 24 hr, **(e-g)** tissue specific expression of target *pGALT9:GUS*, **(e)** control (0 hr), **(f)** 4 hr, **(g)** 24 hr. Error bars indicate standard error ( $\pm$ SE) of three independent experiments. Asterisks indicate significant statistical differences\*\*\*  $P \leq 0.001$ , \*\*  $P \leq 0.01$ , \*  $P \leq 0.05$  using t-test. n=10. Scale bar = 100  $\mu$ m.

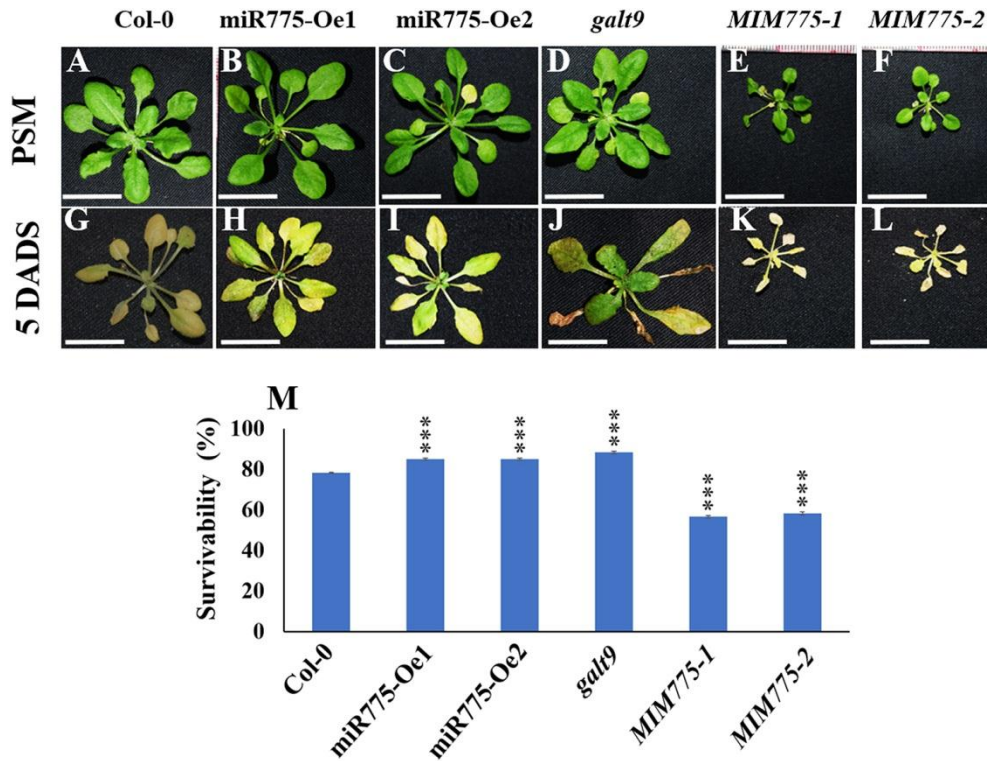


**Figure 6.** Submergence recovery effect in *A. thaliana* by miR775 and its target *GALT9*. (a-f) showing phenotypes in different transgenic lines at pre-submergence (PSM) condition of (a) control (Col-0), (b and c) overexpression lines of miR775 (miR775-Oe1 and miR775-Oe2), (d) target mutant *galt9*, (e and f) target mimic lines of miR775 (*MIM775-1* and *MIM775-2*). (g-l) showing phenotypes of different transgenic lines on 5 days after de-submergence (DADS) of (g) Col-0, (h and i). overexpression lines of miR775 (miR775-Oe1 and miR775-Oe2), (j) target mutant *galt9*, (k and l) target mimic lines of miR775 (*MIM775-1* and *MIM775-2*). (m) showing survivability (%) of different transgenic lines of miR775 along with control (Col-0) on 5 DADS. n=20. 24 hr. Error bars indicate standard error ( $\pm$ SE) of three independent experiments. Asterisks indicate significant statistical differences\*\*\*  $P \leq 0.001$ , \*\*  $P \leq 0.01$ , \*  $P \leq 0.05$  using t-test. n=10. Scale bar = 2.5 cm.

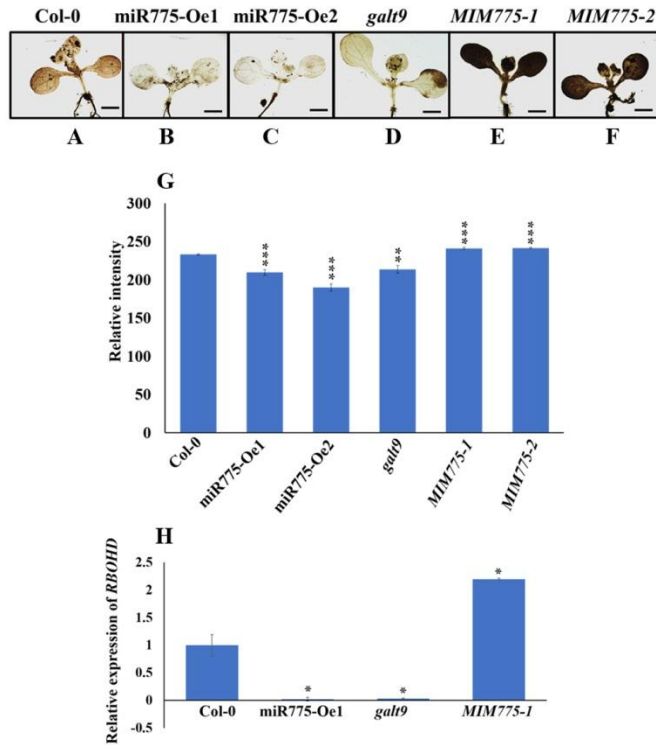


**Figure 7.** Controlled ROS production is essential for recovery signaling. **(a-f)** representative microscopic images of  $H_2O_2$  accumulation (brown color) in 7 dag plant followed by 5 day after submergence **(a)** Col-0, **(b and c)** overexpression lines of miR775 (miR775-Oe1 and miR775-Oe2), **(d)** target *galt9*, **(e and f)** target mimic lines of miR775 (*MIM775-1* and *MIM775-2*), **(g)** quantification of ROS intensity by using ImageJ software, **(h)** relative mRNA abundance of *RBOHD* measured by qRT-PCR in Col-0, miR775-Oe1, *galt9* and *MIM775-1* in rosette leaves at 5 days of post submergence stage. Error bars indicate standard error ( $\pm$ SE) of three independent experiments. Asterisks indicate significant statistical differences \*\*\*  $P \leq 0.001$ , \*\*  $P \leq 0.01$ , \*  $P \leq 0.05$  using t-test.  $n=20$ . Scale bar a-1 = 2 cm and n-s = 100  $\mu$ m respectively.

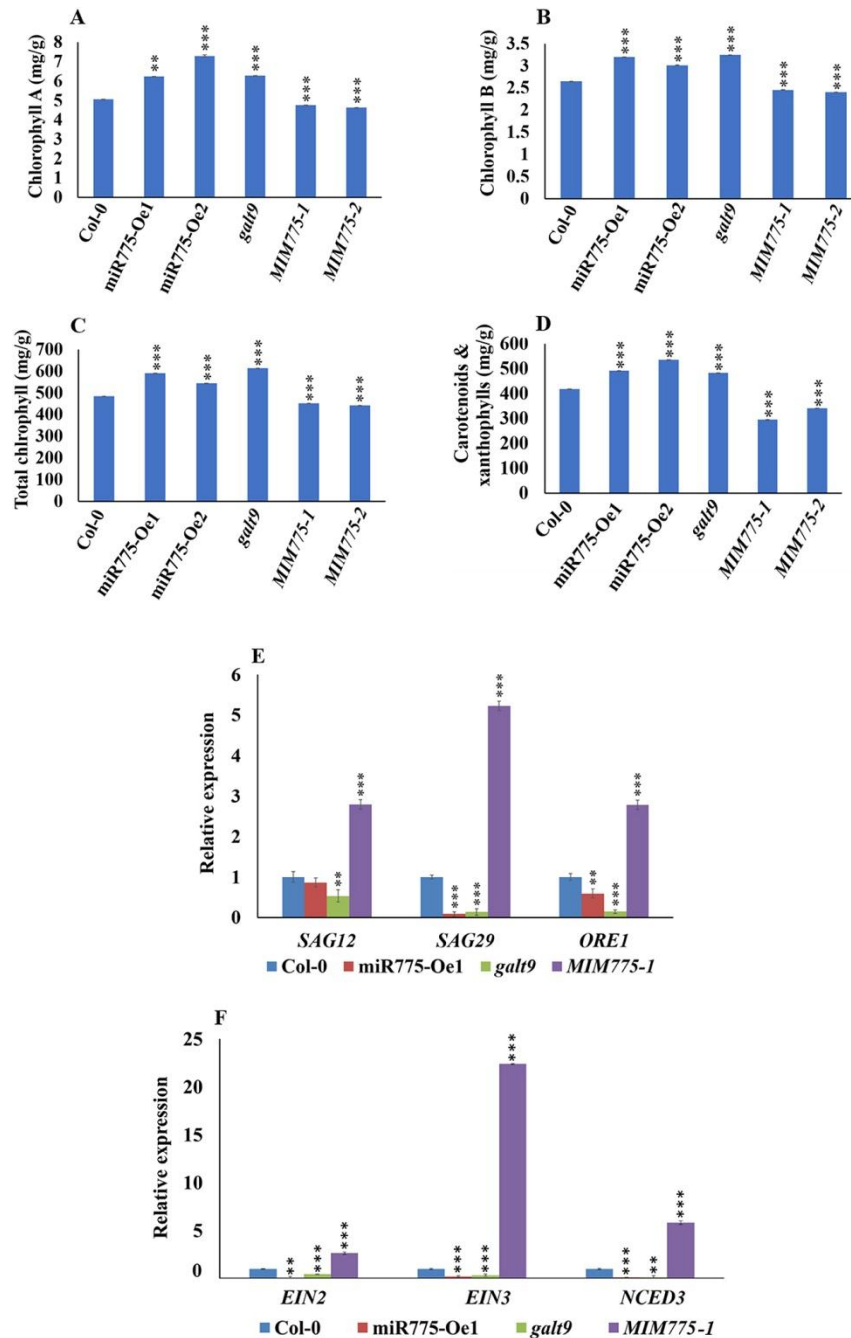


**Figure 8.** Submergence effect on chlorophyll content and expression of senescence associated genes (SAGs). (a, b, c and d) estimation of Chlorophyll A, Chlorophyll B, total Chlorophyll, Carotenoids and Xanthophylls respectively in control Col-0, overexpressing line of miR775-Oe1, *galt9*, and *MIM775-1* of 5days after de-submergence (DADS), (e) Relative expression levels of senescence associated gene (SAG) *SAG12*, *SAG29* & *ORE1* respectively in control Col-0, overexpressing line of miR775 (miR775-Oe-1),

mutant of target *galt9* (*galt9*) and target mimic line of miR775 (*MIM775-1*) of 5 DADS, (f) Relative expression of *EIN2*, *EIN3* and *NCED3*. Error bars indicate standard error ( $\pm$ SE) of two independent experiments for chlorophyll estimation and three independent experiments for relative expression of qRT-PCR. Asterisks indicate significant statistical differences \*\*\*  $P \leq 0.001$ , \*\*  $P \leq 0.01$ , \*  $P \leq 0.05$  using t-test.



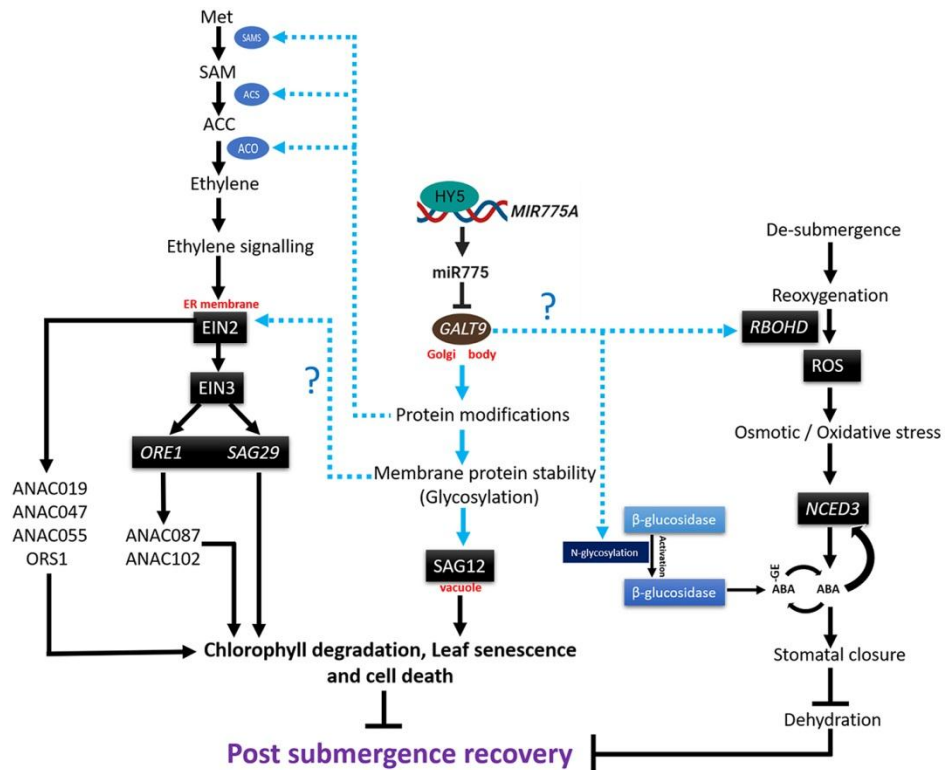


**Figure 9.** Model showing the signalling network mediating post-submergence recovery in *A. thaliana*. The expression of genes changed in our study are highlighted in black-shaded boxes. The solid blue line indicates the possible protein glycosylation through GALT9 during post-submergence recovery. The blue boxes (circular) showing the possible role of GALT9 in N-linked glycosylation of SAM, ACS, and ACO proteins. The N-linked glycosylation of  $\beta$ -glucosidase produces active  $\beta$ -glucosidase (blue rectangle) which catalyzes hydrolysis of glucose-conjugated ABA to produce active ones. Blue dotted line shows the putative role of GALT9, either direct or indirect, in regulation of downstream genes/proteins. GALT9 promotes the expression of EIN2, and thereby downstream EIN3, ORE1, and SAG29. EIN2 is known to promote chlorophyll degradation, leaf senescence, and cell death via ANAC019, ANAC047, ANAC055, and ORS1, whereas *ORE1* does the same via ANAC087 and ANAC102 (Kim *et al.*, 2014). GALT9, by unknown mechanism, induces the expression of RBOHD, which promotes ROS and induces ABA production through induced expression of *NCED3*, and thus affect post-submergence recovery.

(a)

```

Program TSSPlant
Search for RNA II promoters (TSSs) Input file with query sequence(s): /home/apache/tmp/RRhsfX.TSSPlant
Thresholds, for TATA promoters: 1.52
                TATA-less promoters: -0.04
Out of TSSs of different (TATA and TSS-less) classes located at distance 300bp or less, TSS with higher score is selected
Search only on Sense Strand

Query: >Chr1:29421866..29422452
Length of Query sequence: 587
+ chain (TATA-) TSS position: 533 TSS score = 1.8436
+ chain TSS position: 231 TSS score = 1.9844 TATA-box position: 200 TATA-box score = 7.7807
2 promoter(s) predicted
    
```

(b)

		ath-miR775 binding site																														
		**.:** *:* ****: **:******																														
<i>Arabidopsis thaliana</i>	ath-GALT9@NP_175736.2	K	M	A	Q	L	R	R	E	I	A	E	D	I	F	V	L	L	D	I	E	E	E	S	K	L	P	Y	K	T	I	
<i>Arabidopsis lyrata</i>	aly-GALT14@XP_020867175.1	K	M	A	E	L	R	R	E	I	A	E	D	I	F	V	Q	L	D	I	E	E	E	S	K	L	P	Y	K	T	I	
<i>Camelina sativa</i>	csa-GALT14@XP_010500968.1	K	M	A	E	L	R	R	E	I	A	E	D	I	F	V	L	L	D	I	E	E	E	S	K	L	P	Y	K	T	I	
	csa-GALT14@XP_010462209.1	K	M	A	E	L	R	R	E	I	A	E	D	I	F	V	L	L	D	I	E	E	E	S	K	L	P	Y	K	T	I	
<i>Capsella rubella</i>	cru-GALT14@XP_006305251.1	K	M	A	E	L	R	R	E	I	A	E	D	I	F	V	L	L	D	I	E	E	E	S	K	L	P	Y	K	T	I	
<i>Brassica carinata</i>	bca-Hypo@KAG2251403.1	K	M	A	E	L	R	R	E	I	A	E	D	I	F	V	Q	L	D	I	E	E	E	S	K	L	P	Y	K	T	I	
<i>Brassica oleracea</i>	bol-GALT14@XP_013588649.1	K	M	A	E	L	R	R	E	I	A	E	D	I	F	V	Q	L	D	I	E	E	E	S	K	L	P	Y	K	T	I	
<i>Brassica cretica</i>	bcr-Hypo@KAF3515999.1	K	M	A	E	L	R	R	E	I	A	E	D	I	F	V	Q	L	D	I	E	E	E	S	K	L	P	Y	K	T	I	
<i>Brassica napus</i>	bna-Hypo@CDY55849.1	K	M	V	E	L	R	R	E	I	A	E	D	I	F	V	Q	L	D	I	E	E	E	S	K	L	P	Y	K	T	I	
<i>Brassica rapa</i>	bra-Hypo@VDC71021.1	K	M	V	E	L	R	R	E	I	A	E	D	I	F	V	Q	L	D	I	E	E	E	S	K	L	P	Y	K	T	I	
<i>Brassica napus</i>	bna-Hypo@CDY25866.1	K	M	V	E	L	R	R	E	I	A	E	D	I	F	V	Q	L	D	I	E	E	E	S	K	L	P	Y	K	T	I	
<i>Brassica rapa</i>	bra-GALT14@XP_009144780.1	K	M	V	E	L	R	R	E	I	A	E	D	I	F	V	Q	L	D	I	E	E	E	S	K	L	P	Y	K	T	I	
<i>Brassica napus</i>	bna-GALT14@XP_013749000.1	K	M	A	E	L	R	R	E	I	A	E	D	I	F	V	Q	L	D	I	E	E	E	S	K	L	P	Y	K	T	I	
<i>Raphanus sativus</i>	rsa-GALT14@XP_018487292.1	K	M	A	E	L	R	R	E	I	A	E	D	I	F	V	L	L	D	I	E	E	E	S	K	L	P	Y	K	T	I	
<i>Sinapis alba</i>	sal-Hypo@KAF8082308.1	K	M	A	E	L	R	R	E	I	A	E	D	I	F	V	L	L	D	I	E	E	E	S	K	L	P	Y	K	T	I	
<i>Eutrema salsugineum</i>	esa-GALT14@XP_006392804.1	K	M	A	E	L	R	R	E	I	A	E	D	I	F	V	L	L	D	I	E	E	E	S	K	L	P	Y	K	T	I	
<i>Arabis nemorensis</i>	ane-Hypo@VVB00346.1	K	M	V	E	L	R	R	E	I	A	E	D	I	F	I	Q	L	D	I	E	E	E	S	K	L	P	Y	K	T	I	
<i>Arabis alpina</i>	aal-Hypo@KFK35710.1	K	M	A	E	L	R	R	E	I	A	E	D	I	F	I	L	L	D	I	E	E	E	S	K	L	P	Y	K	T	I	
<i>Arabidopsis thaliana</i>	ath-GALT13	K	M	V	E	L	R	S	E	V	A	M	Y	D	I	F	I	L	L	D	I	E	E	E	S	K	L	P	Y	K	T	I

**Fig. S1.** (a) A screenshot of the result of program TSSPlant showing predicted Transcription Start Site (TSS) and TATA-Box, (b) multiple sequence alignment of *GALT9* homologs showing miR775 binding site conservation.

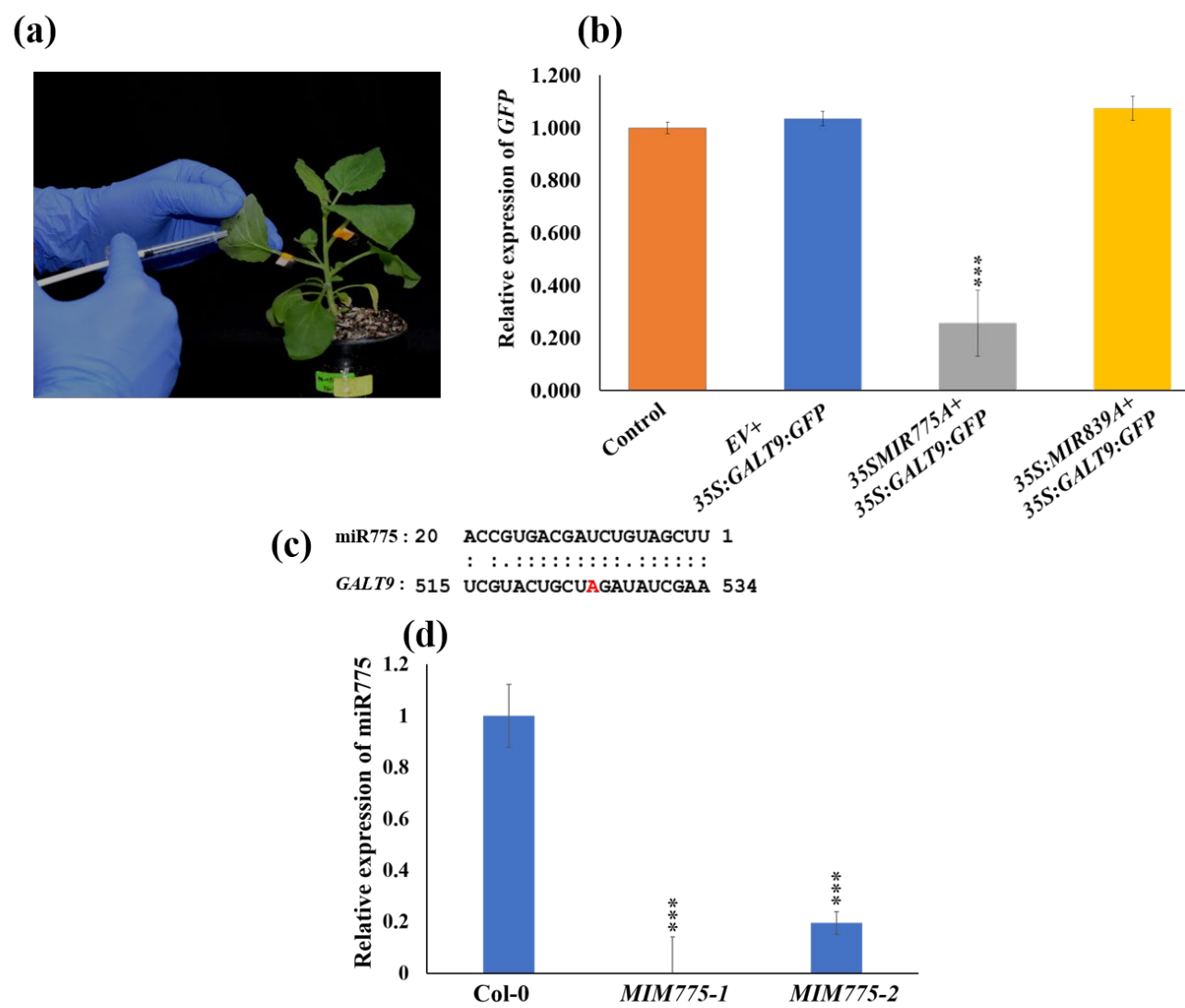


**Fig. S2.** miR775 cleaves its predicted target *GALT9* in a transient assay carried out in tobacco (*N. benthamiana*) leaves. **(a-f)** showing, **(a)** co-infiltration of *MIR775A* and *GALT9* (*35S:MIR775A+35S:GALT9:GFP*) with leaf of tobacco plants (~4 weeks old), **(b)** relative expression level of *GFP* in control (*35S:GALT9:GFP*), *EV+35S:GALT9:GFP*, *35S:MIR775A+35S:GALT9:GFP*, and *35S:MIR839A+35S:GALT9:GFP*, **(c)** sequence alignment of the mature miR775 with the target *GALT9*, **(d)** relative expression of mature miR775 in *MIM775* lines.

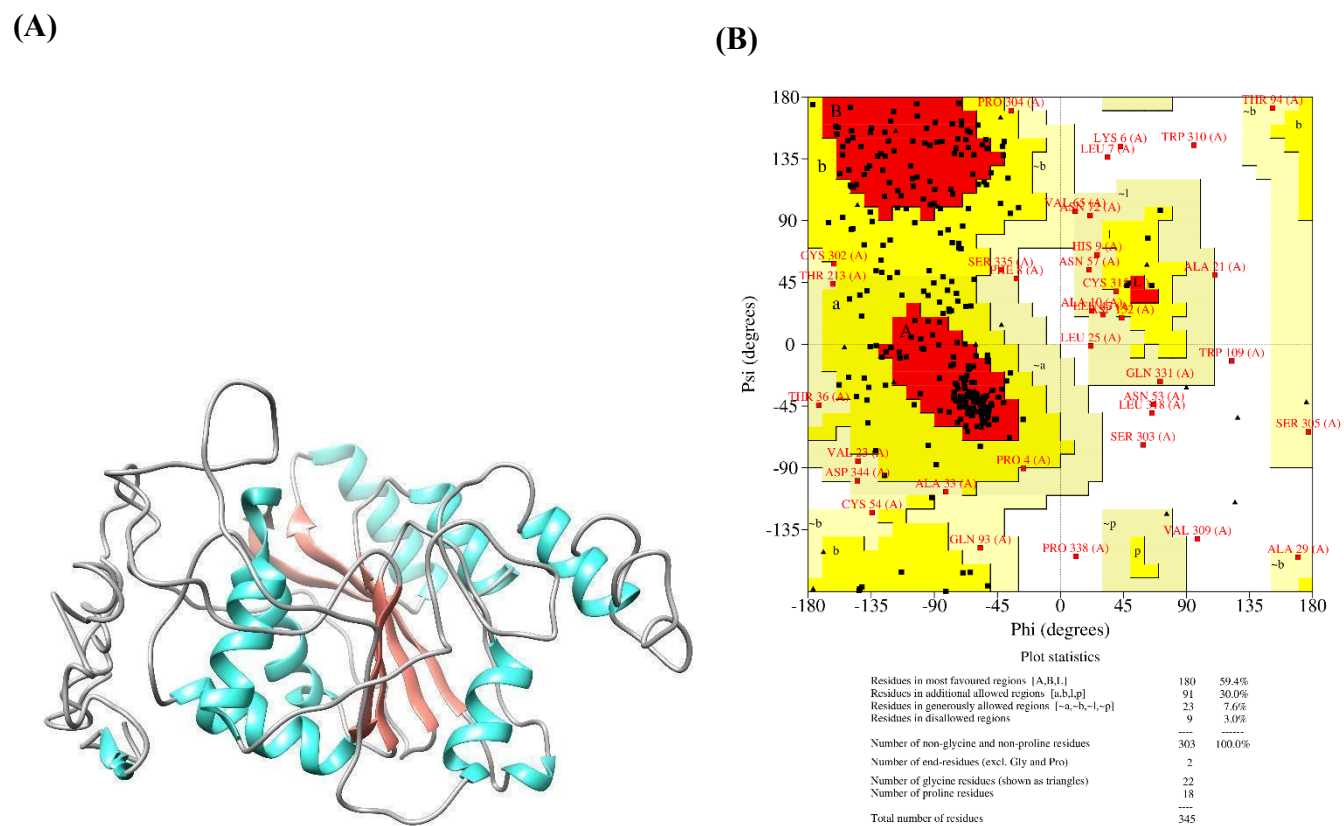


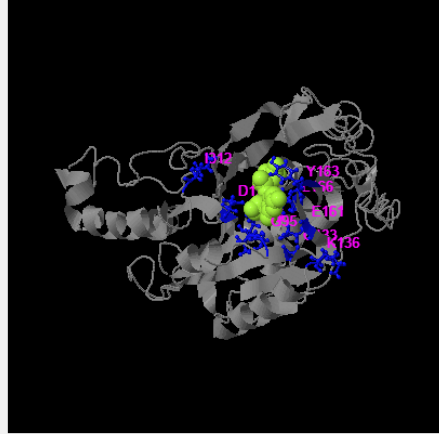
**Fig. S3.** Modeled 3D structure of GALT9 and its quality check. **(a)** Best predicted model of GALT9 through I-TASSER and visualized through UCSF Chimera v1.14. The  $\alpha$ -helix is represented in cyan,  $\beta$ -sheets in brown and the coiled coil in grey, **(b)** stereochemical quality was checked through Ramachandran plot available online at PROCHECK server (<https://saves.mbi.ucla.edu/>), showing 97% of amino acids were in allowed region.

(A)

Predicted function using COFACTOR and COACH

(This section reports biological annotations of the target protein by COFACTOR and COACH based on the I-TASSER structure prediction. While COFACTOR deduces protein functions (ligand-binding sites, EC and GO) using structure comparison and protein-protein network: results (on ligand-binding sites) from the COFACTOR, TM-SITE and S-SITE programs.)

Ligand binding sites



Click to view	Rank	C-score	Cluster size	PDB Hit	Lig Name	Download Complex	Ligand Binding Site Residues
<input checked="" type="radio"/>	1	0.10	11	<a href="#">3otkA</a>	UDP	<a href="#">Rep.</a> <a href="#">Mult.</a>	93,94,95,133,136,161,163,166,190,312
<input type="radio"/>	2	0.08	9	<a href="#">2AM3A</a>	<a href="#">2AM3A00</a>	<a href="#">Rep.</a> <a href="#">Mult.</a>	93,94,160,161,162,163,165,166,169,231,274,275,276,277
<input type="radio"/>	3	0.07	7	<a href="#">2j0bA</a>	UDP	<a href="#">Rep.</a> <a href="#">Mult.</a>	93,94,95,98,101,169,190,191,192,311
<input type="radio"/>	4	0.03	3	<a href="#">5ej1A</a>	BGC	<a href="#">Rep.</a> <a href="#">Mult.</a>	166,190,248,275,277
<input type="radio"/>	5	0.03	3	<a href="#">2FFUA</a>	<a href="#">2FFUA00</a>	<a href="#">Rep.</a> <a href="#">Mult.</a>	163,228,229,230,231,248,249,298,299,300,301,311,344

[Download](#) the residue-specific ligand binding probability, which is estimated by SVM.  
[Download](#) the all possible binding ligands and detailed prediction summary.  
[Download](#) the templates clustering results.  
 (a) C-score is the confidence score of the prediction. C-score ranges [0-1], where a higher score indicates a more reliable prediction.  
 (b) Cluster size is the total number of templates in a cluster.  
 (c) Lig Name is name of possible binding ligand. Click the name to view its information in [the BioLiP database](#).  
 (d) Rep is a single complex structure with the most representative ligand in the cluster, i.e., the one listed in the Lig Name column. Mult is the complex structures with all potential binding ligands in the cluster.

Spin On/Off

(B)

**Receptor Information**

PDB ID: [3otk](#)  
 Chain: A  
 Resolution: 2.3 Å  
 UniProt ID: [Q99324](#) (Beta-1,3-galactosyl-0-glycosyl-glycoprotein beta-1,6-N-acetylglucosaminyltransferase)

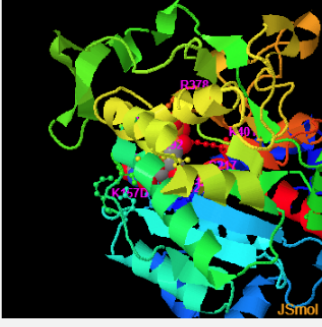
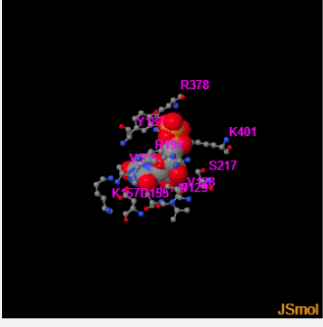
**Ligand Binding/Catalytic Sites**

ID	Name (Show Synonyms)	Chemaxon Viewer	Binding Affinity
<a href="#">UDP</a>	URIDINE-DIPHOSPHATE	The version number of the Java plugin is lower than 1.6. Current Marvin requires at least version 1.6.	

Global View, download [receptor](#), [ligand](#)

Local View

Ligand-Protein Interaction

spin

Catalytic Site Residues: N/A

**Enzyme Commission**

EC Number: [2.4.1.102](#)  
 Name: Beta-1,3-galactosyl-0-glycosyl-glycoprotein beta-1,6-N-acetylglucosaminyltransferase

**Gene Ontology**

GO Terms	Name
<a href="#">GO:0000139</a>	Golgi membrane
<a href="#">GO:0003829</a>	beta-1,3-galactosyl-0-glycosyl-glycoprotein beta-1,6-N-acetylglucosaminyltransferase activity
<a href="#">GO:0005794</a>	Golgi apparatus
<a href="#">GO:0006486</a>	protein glycosylation
<a href="#">GO:0008375</a>	acetylglucosaminyltransferase activity
<a href="#">GO:0016020</a>	membrane
<a href="#">GO:0016021</a>	integral to membrane
<a href="#">GO:0016740</a>	transferase activity
<a href="#">GO:0016757</a>	transferase activity, transferring glycosyl groups
<a href="#">GO:0048729</a>	tissue morphogenesis
<a href="#">GO:0060993</a>	kidney morphogenesis

**Fig. S4. (a)** Screenshot of I-TASSER result showing predicted biological annotation of GALT9, **(b)** Screenshot of BioLiP (biologically relevant ligand-protein binding interactions) database showing the Function Annotation of 3otk, which is a significant PDB hit of predicted GALT9 3D structure.

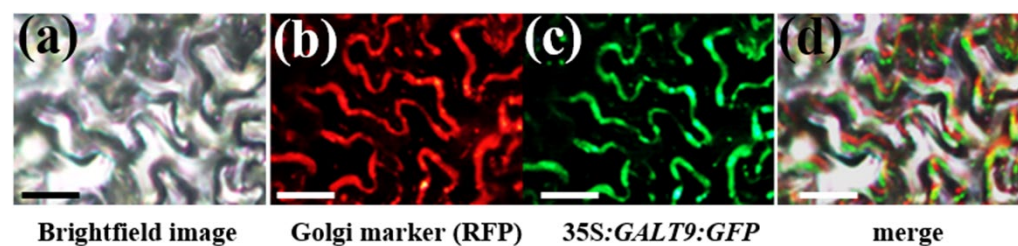
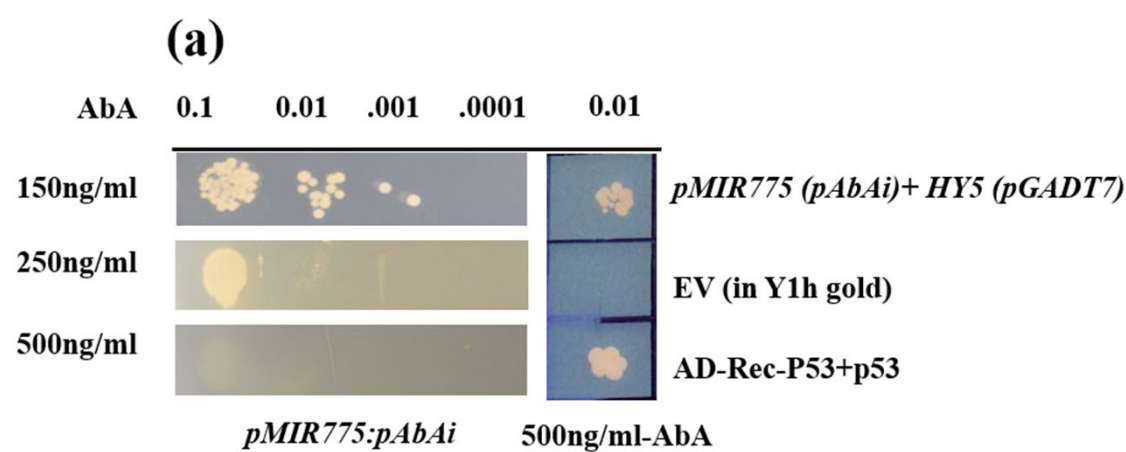


**Fig. S5.** GALT9 localizes in the Golgi apparatus of a cell. **(a to d)** the fluorescent protein-tagged GALT9 fusion proteins were co-expressed with GmManI-pBIN2 (mCherry Golgi apparatus marker) into the abaxial side of a young tobacco (*N. benthamiana*) leaf epidermis. The signals were visualized under a fluorescence microscope. **(a)** Bright field image of leaf epidermal cells, **(b)** fluorescence image of *GmManI-pBIN2* (Golgi apparatus marker), **(c)** fluorescence image of *35S:GALT9:GFP*, **(d)** image was merged with fluorescence image of GmManI-pBIN2 and *35S:GALT9:GFP*. Scale bar = 50  $\mu$ m.



Determination of autoinhibition of AbA, plated on SD-URA plate

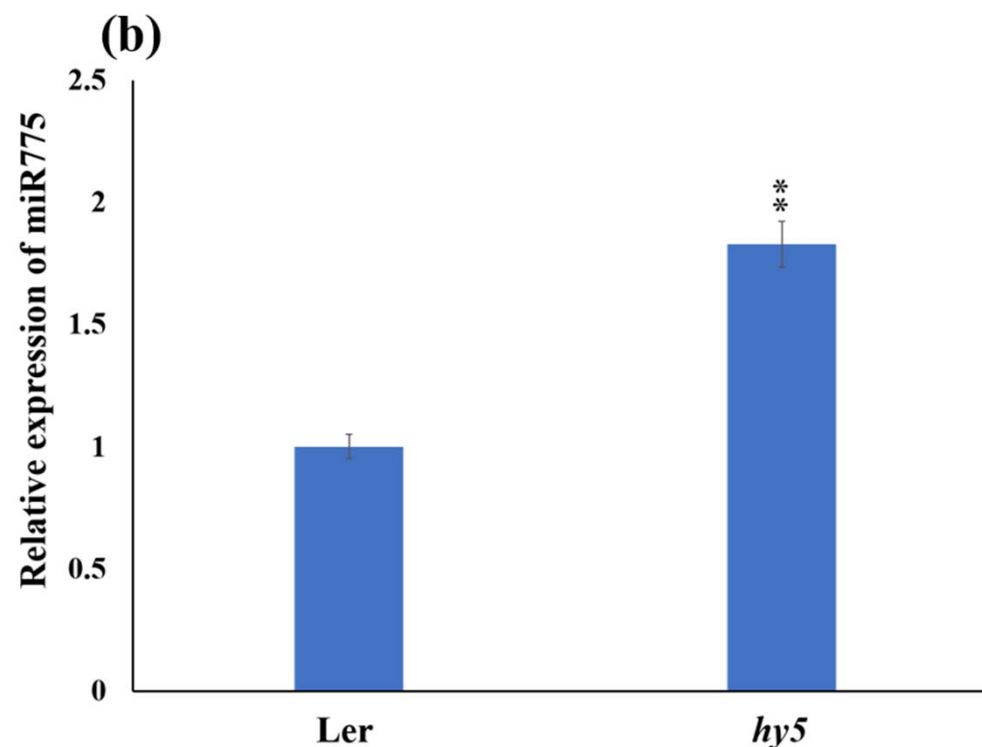


**Fig. S6.** HY5 binds to the promoter of *MIR775A* and regulates its expression. **(a- b)**, **(a)** determination of autoactivation, represents Yeast one hybrid (Y1H) assay showing the interaction of HY5 with *pMIR775A*. *HY5* CDS + *pGADT7* transformed into *pMIR775A* + pAbAi was used to check the interaction. *pGADT7-Rec-p53/p53-AbAi* was used as a positive control. *pGADT7* transformed into a Y1H gold cell used a negative control, **(b)** expression of miR775 in *hy5* mutant background.

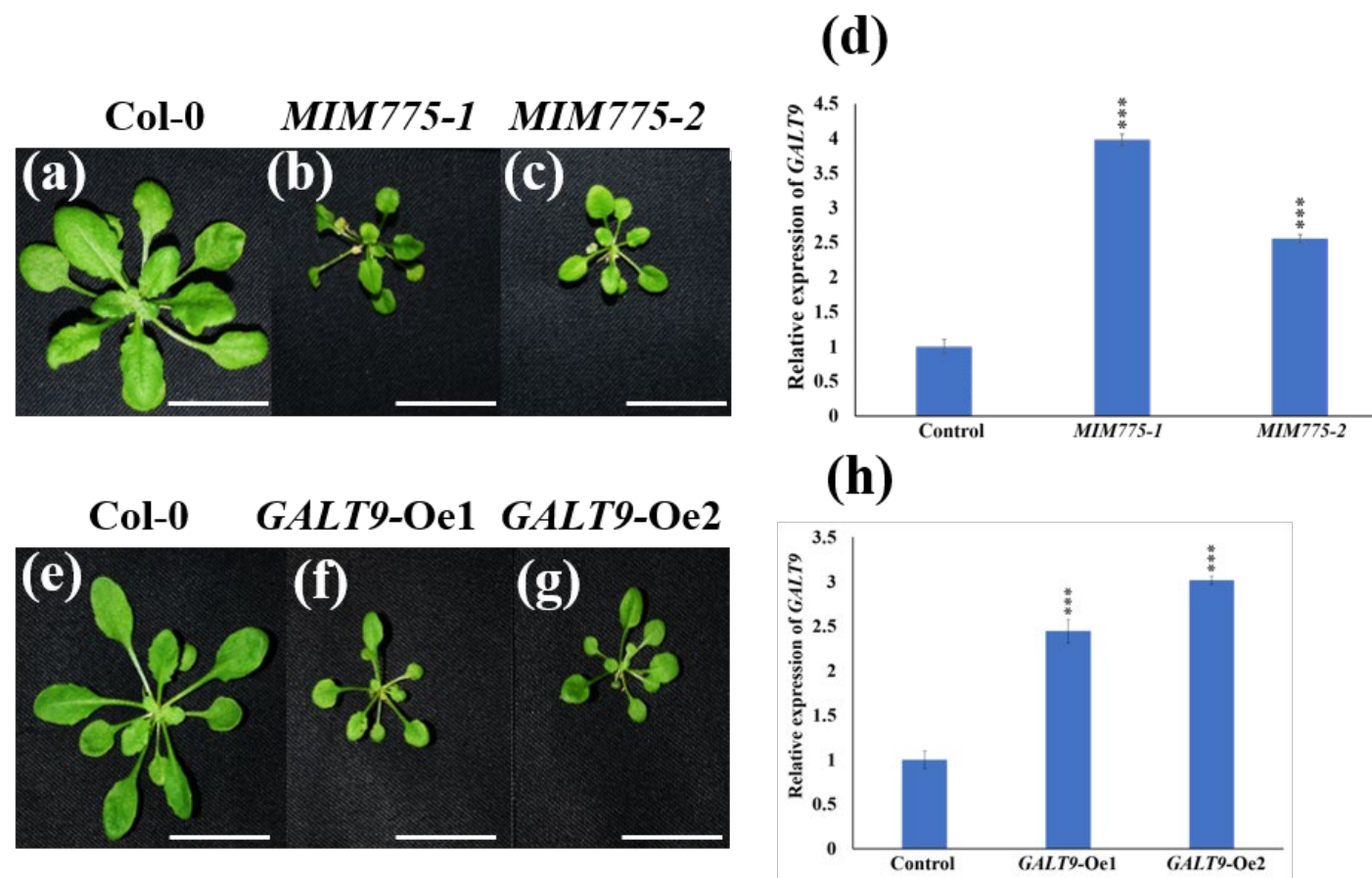


**Fig. S7.** Phenotypic comparison of *MIM775* and *GALT9* regulating leaf sizes in *A. thaliana* (a-c) phenotypic comparison of *MIM775* in two independent lines of *MIM775* (*MIM775-1*, *MIM775-2*), (d) relative expression of *GALT9* in two independent lines *MIM775-1* and *MIM775-2* (e-g) phenotypic comparison of *GALT9* in two independent lines of *GALT9* overexpression (*GALT9-Oe1* and *GALT9-Oe2*), (h) relative expression of *GALT9* in two independent lines of *GALT9-Oe1* and *GALT9-Oe2*. Scale bar= 2.5 cm.

**Table S1.** List of probable targets of miR775 validated through cleaveland software using degradome PARE data of 11-days seedling (SRR3143654)

[Click here to download Table S1](#)

**Table S2.** List of probable targets of miR775 validated through cleaveland software using degradome PARE data of Sample leaf of stage 5 (SRR3143654)

[Click here to download Table S2](#)

**Table S3.** List of primers used in the study

[Click here to download Table S3](#)

**Table S4.** List of Coexpressed gene with *GALT9*

[Click here to download Table S4](#)